Society for Science and Education
United Kingdom

ISSN: 2055 - 1266
Volume 2. Issue 1

Journal of Biomedical Engineering and Medical Imaging

TABLE OF CONTENTS

EDITORIAL ADVISORY BOARD

DISCLAIMER

All the contributions are published in good faith and intentions to promote and encourage research activities around the globe. The contributions are property of their respective authors/owners and the journal is not responsible for any content that hurts someone's views or feelings etc.

SOCIETY FOR SCIENCE AND EDUCATION UNITED KINGDOM

JBEMi JOURNAL OF BIOMEDICAL ENGINEERING AND MEDICAL IMAGING

ISSN: 2055-1266
VOLUME 2 ISSUE 1

What is the New Tumor Marker for Detection of Different Kidney Tumors? Modern Study to Isolation, Purification, and Characterization of Galactose Binding Lectin from Sera of Patients with Kidney Cancer

Rasha Hasan Jasim[1], Hathama Razooki Hasan[2] and Majed Khadum Husain[3]
[1]*Chemistry Department, College of Education for Girls, University of Kufa*
[2]*Chemistry Department, College of Science, University of Baghdad*
[3]*Biochemistry Department, College of Medicine, University of Kufa. IRAQ*
dr.rashahussainee@yahoo.com

ABSTRACT

The present study was designed to investigate lectins in sera of patients with kidney tumors, in addition to non tumoral kidney disease patients. Fifty five patients of malignant kidney tumors were enrolled in addition to 23 patients of benign kidney tumors, and 18 patients of non tumoral kidney diseases used as control groups, in addition to 46 healthy individuals were also investigated. The age of patients and healthy individuals were 10-90 years. The measurement of total serum proteins revealed significant ($p < 0.001$) decrease in patients of malignant tumors when compared with those of benign, non tumoral diseases, and healthy individuals. The conditions of the hemagglutination assay of serum lectin activity were optimized. They were Tris buffer of 20 mM and pH 7.4, 60 mM $CaCl_2$, 800 µg of defatted serum, 30 ˚C for serum samples, 60 minutes for serum samples, and human blood of group A^+ suspension with 1.4 optical density. The measurement of the specific hemagglutination activity of lectins demonstrated significant ($p < 0.001$) elevation in patients of malignant tumors when compared with those of other patients and healthy individuals. Lectin activity was pointed out to be significantly ($r = 0.767$ at $p < 0.0005$) positively correlated with stage of malignancies. The cutoff value of the specific hemagglutination activity was found to equal 6 SHU for discriminatory malignant kidney tumors. Serum lectins activity were indicated to be inhibited by galactose, mannose, lactose, and N-acetyl galactosamine. Purification of lectin from sera of patients with malignant kidney tumors by affinity chromatography with the use of silver stain revealed galactose binding lectin (GalBL). The purified folds and the yield was 132 with 22.1. The polyacrylamide gel electrophoresis (PAGE) of purified lectin demonstrated one band consisted lectin activity. The approximate molecular weight of GalBL was determined and found to be 98.40. Purified lectin was characterized through the assessment of the capability to agglutinate RBCs, inhibition by EDTA, pH dependency, thermal dependent, and carbohydrate contents. GalBL was observed to be calcium independence lectins. These results suggest that the diagnosis of the specific hemagglutination activity of lectin is a promising biomarker for

DOI: 10.14738/jbemi.21.702
Publication Date: 2nd February 2015
URL: http://dx.doi.org/10.14738/jbemi. 21.702

discrimination of malignant kidney tumor patients and the purified lectin could be introduced in the field of biomarkers.

Key Word: lectin, kidney, cancer, galactose, tumor, purification

1 Introduction:

Lectins was first discovered as a highly toxic protein that was isolated from castor tree seeds (Ricinus communis), and named ricin [1], this protein showed the ability to agglutinin erythrocytes [2]. In 1888; Peter Hermann Stillmark, had called this protein as hemagglutinin, or phytoagglutinin, because it was originally found in the extracts of some plants [3- 5]. Kilpatrick [6], Houzelstein et al [7], and Naird et al [8] reported that the lectin was first discovered in snake by Mitchell W in 1860. Mitchell and Stewart described red blood cell agglutination by snake venom in 1883, although this term was not used at that time [6]. Furthermore, in 1886 they published the first study dealed with lectin activity [9, 10]**.** Because of the variation in lectins types, their chemical and physical properties, their roles and applications in the different species were varied too [see reference 11]. Lectins provide way for one molecule to stick to another one without any immunity involved.

They play a wide role in health, but their ability to influence the inflammatory process indicates that they are involved in inflammatory diseases, e.g.: bowel disease, systematic lupus erythematosus, rheumatoid arthritis, and even weight gain [12-15]. Majority of lectin researches have focused on the using of lectins from different sources (other than human) in human medical fields. Somewhat, working with human lectins was surrounded by difficulties, as a result of that, human endogenous lectins studies were, rather, few [16-18].

In human, some lectin genes are expressed constitutively, whereas others are induced by gene activation under specific biological circumstances [19]. Membrane-bound and many soluble lectins are synthesized on ER-bound ribosomes and delivered to their eventual destinations via the ER-Golgi pathway. However, a significant subset of soluble lectins (galectins, heparin-binding growth factors, and some cytokines) are synthesized on free ribosomes and delivered directly to the exterior of the cell by a poorly understood mechanism involving extrusion through the plasma membrane. Some of these lectins can recognize biosynthetic intermediates that occur in the Golgi-ER pathway (e.g., galactosides and high-mannose oligosaccharides) [20].

There are no reliable tumor markers that can be used in the diagnosis, treatment, screening of patients with renal cell carcinoma (RCC) [21], till now general tumor markers in RCCs has been used to assess a cancer's response to treatment and to check for cancer recurrence [22]. Generally, renal cancer is the third most common malignancy of the genitourinary system, and accounts for 3% of adult malignancies globally [23]. The incidence of RCC has been increasing 2 to 4% per year since the 1970s, perhaps related in part to the improvement in and increased use of modern imaging techniques [24]. Limited early warning signs result in late recognition with metastases present in approximately one third of patients at the time of diagnosis, with 210,000 new cases per year and more than 100,000 deaths occurring worldwide annually [25]. The male to female ratio is 1.5:1, and the disease usually occurs in the sixth and seventh decades of life [26]. RCCs are highly vascularized tumors, which may explain the 30-40% prevalence of metastatic disease at initial diagnosis [27], when systemic therapies are then necessary. In

this group of patients, one-year survival rate are ~ 25%, illustrating the limited role of both chemotherapy and radiotherapy in the management of advanced stages of RCC [28]. Advanced RCC responds poorly to systemic therapy and has a 5 year survival rate of less than 10% [23]. Defining the prognosis of RCC is important for both therapeutic decision-making and counseling patients. The prognosis is heavily affected by the extent of disease; the best treatment results can be anticipated in those with minimal tumor spread [29].

2 Materials and methods

Patient and Control Individuals: The present study involved 96 patients (55 cases with malignant kidney tumors, 23 cases with benign kidney tumors, and 18 cases with non tumoral kidney diseases) with the age range 10-80 years, in addition to 46 healthy individuals, at the same age range. The enrolled patients were attended: Al - Sadder Medical City, Al - Ameer Private Hospital, and Al - Ghadeer Private Hospital in Najaf. The diagnosis was confirmed by histopathological examination. Healthy individuals were nonsmokers and they were not subjected to surgical operation.

Serum Samples: Ten milliliters of venous blood samples were collected from patients and the control groups. Samples were allowed to clot at room temperature, centrifuged at 3000 xg for 5 minutes, then sera were collected and stored at -20˚C.

Isolation of Crude Lectins from Serum and Tissue Specimens: Ten milliliters of venous blood samples were collected from patients and the control groups. Samples were allowed to clot at room temperature, centrifuged at 3000 xg for 5 minutes, and then sera were collected and stored at –15˚C.

For isolation of serum crude lectins, 1 volume of serum was mixed with 2.5 volumes of petroleum ether, the mixture was shacked strongly, then, centrifuged at 3000 xg for 5 minutes. The organic phase was neglected and defatted serum was stored at -20˚C to be used for determination of the hemagglutination activity.

Preparation of Standard Ttrypsinized Erythrocyte Suspension for Hemagglutination Test: Human blood group erythrocytes were collected from the local blood bank in Al-Sadder Medical City in Najaf Government in Iraq. Blood was centrifuged at 3000 xg for 5 minutes, the sera were discarded. The erythrocytes were washed with saline solution (5 ml saline: 1 ml packed erythrocytes), then were suspended in phosphate buffer saline solution (pH 7.4), and diluted with the same buffer to give an absorbance of 2 ml at 620 nm.

One part of trypsin solution (1%) was added to 10 parts of the final erythrocytes suspension. the mixture was incubated at 37˚C for 1 hour, and then centrifuged at 5000 xg for 5 minutes. The trypsinized erythrocytes mixture was washed 3 – 5 times with saline solution to remove trypsin traces. Saline solution was added, until the absorbance of the erythrocyte suspension was 1.4 at 620 nm.

Protein Determination: Total proteins in the studied samples were estimated using Bradford method [30], and bovine serum albumin was used as a standard protein.

Determination of Hemagglutination Activity of Crude Serum and Tissue Lectins of Patient and Control Groups: To determine the hemagglutination activity in serum and tissue Lis and Sharon [2] method was used, with essential modifications. The procedure involved three tubes, test (T), blank (B), and control (C). A set of control tubes (2 – 4) were used in each experiment and the assay was carried out as in the

following: The reduction of optical density (ROD) in the test tube (in crude sera and tissues determination) was measured from the following equation:

$$ROD\% = \frac{A_C - A_{T-B}}{A_C} \times 100 \quad (1)$$

Where: A_C: Optical density of cell suspension in the control tube. A_{T-B}: Optical density of cell suspension in the test tube – Optical density of cell suspension in the blank tube. Specific hemagglutination activity unit (SHU) was expressed as hemagglutination units per milligram of protein.

Purification of GalBL: Affinity chromatography technique was applied for the purification of GalBL from patients' with malignant kidney tumors. Preparation of the affinity chromatography column was carried out according to the instructions of Hermanson [31], and Amersham handbook [Amersham Pharmacia Biotech].

Determination of Carbohydrate Content in the Purified GalBL: Dubois method [32] was followed for determination of carbohydrate amount in the purified GalBL. Where glucose was used as a standard sugar.

3 Results and Discussion

Levels of the Specific Hemagglutination Activity in Patients and Control Groups: The optimized conditions of the hemagglutination protocol were used for estimation of individual serum lectin activity in the studied groups. It was expressed as SHU. Figure 1, demonstrates that 52 patients out of the 55 studied patients of malignant kidney tumors have a hemagglutination activity higher than 6 SHU, while those of non tumoral kidney diseases and healthy individuals (except one sample in each group) have less than 6 SHU. Also those of benign kidney tumors were found to have specific activity less than 6 SHU. These results suggest the possibility of using 6 SHU as a cutoff value for the specific hemagglutination activity. A result showed the possibility of using this parameter as a biomarker for discriminating of patients with malignant kidney tumors among those with benign, non tumoral kidney diseases, and healthy individuals.

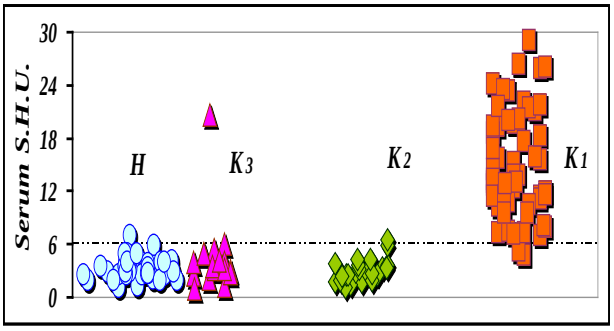

Figure 1: Distribution of the Serum Hemagglutination Activity in Patients of Malignant Kidney Tumors (K_1), Benign Kidney Tumors (K_2), Non Tumoral Kidney Diseases (K_3), and Healthy Individuals (H). The symbol – - – - refer to the cutoff of malignant kidney tumors

The evaluation of the specific hemagglutination activity in the various groups revealed a significant increase ($p < 0.001$) in patients of malignant kidney tumors when compared with those of benign tumors, non tumoral kidney diseases, and healthy individuals. However, non significant variations were obtained when other groups were compared together (table 1). The sensitivity and specificity of serum lectin activity in detection of malignant kidney tumors were 94.54 % and 95.65 % respectively.

Table 1: Serum Specific Hemagglutination Activity Levels in Patients of Malignant Kidney (K_1) and Benign Kidney (K_2) Tumors, Non Tumoral Kidney Diseases (K_3), and Healthy Individuals (HK_1 and HK_2)

Groups	Age (year) Mean ± S.D. Range	SHU Mean ± S.D.	Range	*p*
K_1 (55)	54.93 ± 12.50 32 – 80	14.99 ± 6.21	4.79 – 29.08	0.000** for K_1 vs K_2 0.000** for K_1 vs K_3 0.309 for K_2 vs K_3 0.000** for K_1 vs H_{K1} 0.491 for K_2 vs H_{K2} 0.724 for K_3 vs H_{K2}
K_2 (23)	45.04 ± 15.33 10 – 66	3.04 ± 1.31	1.17 – 6.49	
K_3 (18)	42.39 ± 16.60 12 – 68	4.44 ± 4.27	0.99 – 20.70	
H_{K1} (32)	47.38 ± 10.92 32 – 80	4.27 ± 1.87	1.09 – 9.09	
H_{K2} (43)	39.77 ± 13.77 10 – 66	3.94 ± 1.71	1.09 – 9.09	

*The mean difference is significant at the 0.001 level. **Refers to significant difference between variables.*

Implication of Stages of Malignancy in Serum and Tissue Specific Hemagglutination Activity: In order to verify the changes of the hemagglutination activity with the advancing of malignancy, the patients were subdivided according to the stage of the diseases into stage I, II, III, and IV. From the statistical analysis of the malignant kidney tumors of different stages, a positive correlation was observed between the serum specific hemagglutination activity & the malignant tumor progression ($r = 0.767$ at $p < 0.0005$) (Figure 2).

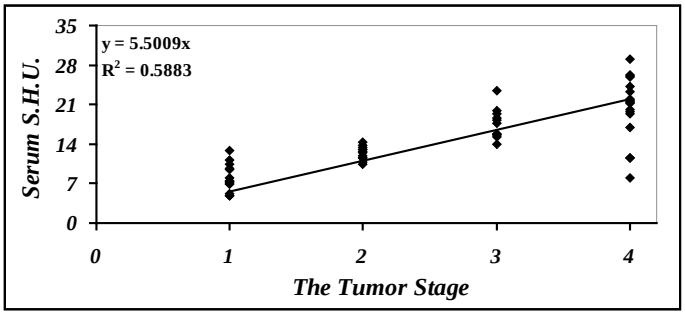

Figure 2: Correlation of Serum Hemagglutination Activity with Stages of Malignant Kidney *Tumors*

The mean levels of specific hemagglutination activity in patients of the four stages of malignant kidney tumors are illustrated in table 2. Significant elevations ($p < 0.001$) of the specific hemagglutination activity were observed when the data of each two stages (except III and IV) were compared.

Table 2: Stage Differences in Serum Specific Hemagglutination Activity of Malignant Kidney Tumor Patients

Subjects	Age (year) Mean± S.D. Range	SHU Mean± S.D.	Range	*p*
Stage I (14)	*49.07 ± 11.94 32 – 74*	*8.03 ± 2.40*	*4.79 – 12.80*	*0.000** For (1, 2, 3, 4, and 5) 0.011 for (6)*
Stage П (12)	*55.67 ± 13.85 34 – 79*	*12.40 ± 1.21*	*10.37 – 14.42*	
Stage Ш (11)	*53.73 ± 9.71 43 – 75*	*17.58 ± 2.73*	*13.87 – 23.47*	
Stage IV (18)	*59.72 ± 12.40 41 – 80*	*20.55 ± 5.57*	*7.97 – 29.08*	

*The mean difference is significant at the 0.001 level. **Refers to significance between the variables. 1)Stage I vs. Stage II, 2) Stage I vs. Stage III, 3) Stage I vs. Stage IV, 4) Stage II vs. Stage III, 5) Stage II vs. Stage IV 6) Stage III vs. Stage IV*

Gender Involvement in Kidney Lectins Hemagglutination Activity Changes: The effect of gender on the kidney specific hemagglutination activity levels in patients of cancerous tumors, benign tumors, and non tumoral kidney subgroups was evaluated. **Student's *t-test*** failed to exhibit significant changes among male and female patients (Table 3).

Table 3: Gender Differences of Serum Specific Hemagglutination Activity in Tumoral and non Tumoral Kidney Disease Patients and Healthy Individuals

Type	Gender	Age (year) Mean ± S.D. Range	SHU Mean ± S.D.	Range	*p*
K_1 (55)	M (36)	*57.31 ± 13.69 32 – 80*	*15.48 ± 6.94*	*4.79 – 29.08*	*0.259*
	F (19)	*50.79 ± 9.19 37 – 65*	*14.08 ± 4.55*	*7.97 – 21.69*	
K_2 (23)	M (14)	*43.93± 16.73 10 – 66*	*2.40 ± 0.77*	*1.17 – 3.59*	*0.377*
	F (9)	*47.44 ± 12.28 25 – 62*	*4.04± 1.38*	*2.45 – 6.49*	
K_3 (18)	M (11)	*47.36 ± 11.33 27 – 62*	*3.95 ± 1.23*	*2.05 – 6.00*	*0.550*
	F (7)	*34.57 ± 21.22 12 – 68*	*5.21 ± 6.92*	*0.99– 20.70*	
H (46)	M (21)	*44.24 ± 9.57 10 -81*	*4.69 ± 2.08*	*1.09– 9.09*	*0.432*
	F (25)	*44.88 ± 17.10 11– 87*	*3.53 ± 1.14*	*1.09 – 6.13*	

K_1:Malignant Kidney Tumor Patient group, K_2: Benign Kidney Tumor Patient group, K_3: Non Tumoral Kidney Patients, and H: total healthy individuals. M: Male, F: Female. The mean difference is significant at 0.001 level

Previously, the source of increased serum lectins in cancer patient was reported to be unclear [33]. The significant positive correlations of serum and tissue lectins of patients with malignant tumors reported here suggest presence of a direct relationship between their lectins levels which means that the malignant tumors are the sources of lectin present in the sera of the malignant patients [data not shown].

In the present study, removal of the tumors, decreased serum hemagglutination activity, thus tumor tissues are most likely to produce and secrete lectins in sera. The agglutination test of cancerous tissues showed that lectin was found not only on malignant cells but also in macrophages and stromal cells (mainly fibroblasts) near cancer focus, and the stromal cells immediately adjacent to cancer nests was found to have higher levels of the hemagglutination activity in comparison to cells far from the nests. These results suggest that circulating lectins are generated not only by tumor cells but also from peritumoral inflammatory cells and stromal cells. Different modalities have been proposed to explain how lectins might be involved in the metastatic process: (1) Lectins act as a bridge molecule enhancing the adhesive interactions between tumor cells and the extracellular matrix. (2) Several lectins are able to mediate homotypic cell-cell adhesion through interaction with complementary glycoproteins depending on the hypothesis that lectins are involved in the formation of tumor emboli and dissemination of tumor cells in the circulation. (3) Lectins are able to protect the malignant cell against apoptosis induced by the loss of cell anchorage. The expression of lectins in tumor cells may provide a critical determinant for cell survival of disseminating cancer cells in the circulation during metastasis [33].

In patients with benign tumors serum hemagglutination activity was found to remain within values of healthy individuals, this is due to the differences of benign from malignant tumors. In contrast to the malignant cells, benign tumor cells are under control. On the other hand, during benign tumor formation, several lectins, which extend normally on the cell surface, are degraded and others are built, these processes are contributed in keeping lectin concentration balance [34].

Various lectins from different species are studied for evaluation of their roles in cancer treatment, and therapy. Preliminary findings suggest that some lectins, but not all; can detect alterations of malignant cells as well as reduce the cancer cell tumorigenicity, thus may have benefits for the immune status of the patients. A lectin from Viscum album (mistletoe) for instance is known to increase the reactivity of the lymphocytes of tumor-bearing mice to the mitogens *in vitro*, thus indicating its immune stimulating effects for cancer-immunosuppressed lymphocytes. It also inhibits the protein synthesis in various malignant cell lines. Similarly, because of the cytostatic/apoptotic and immunomodulatory effects of the mistletoe lectin, the extracts are often applied in the treatment of tumor bearing patient [20].

Purification of Serum Human Gal BL: Hydrophobic affinity chromatography was used for isolation and purification of galactose binding lectin from sera of patients with malignant kidney tumors, benign kidney tumors, non tumoral kidney diseases, and healthy individuals. The purification protocol was carried out by using sepharose 6B column activated with bis-oxirane (1, 4 – Butanediol diglycidyl ether) ($C_{10}H_{18}O_4$). The chromatograms of the purified lectins was demonstrated in figures 3. The purification folds and the yield percentage of GalBL was 132 with 22.1 % (table 4).

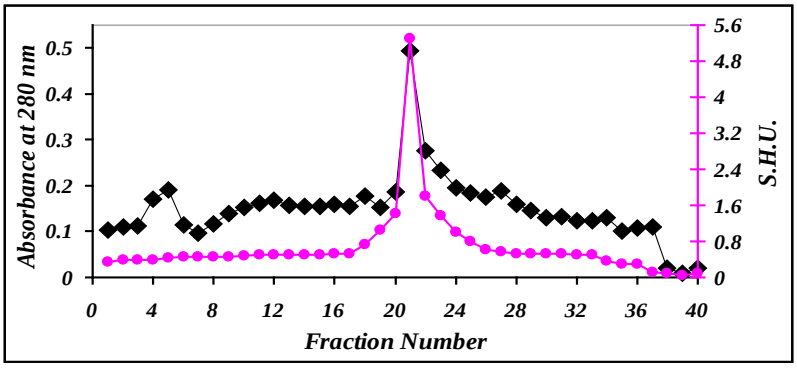

Figure 3: Affinity Chromatogram of Malignant Galactose Binding Lectin (GalBL) using Sepharose 6B // Galactose Column (1.6×1.3) at Flow Rate 30ml / hour. The volume of each fraction was 1ml.Tris Buffer 20 mM and 7.4 pH was used as a Washing Solution. The Elution step was carried out using a Tris Buffer (20 mM, pH 7.4) contained 30 mM Galactose.

Table 4: Results of the Purification Protocol of Lectins from Sera of Patients with Malignant Kidney Tumors

Purification step	Total volume (ml)	Total protein (mg)	Total activity (HU)	SHU (HA/µg of protein)	Purification (fold)	Yield %
MKT Serum	3	45	44.325	0.985	1	100
GalBL	5	0.0750	9.783	130.440	132	22.1

MKT: Malignant Kidney Tumor Serum; GalBL: Galactose Binding Lectin

The purification protocol was applied for the analysis of sera from patients with benign kidney tumors and non tumoral kidney diseases, in addition to healthy individuals, sera of the three groups of enrolled individuals failed to appear same malignant sample results.

In various lectin studies, “conventional” procedures including salt-induced crystallization, ethanol precipitation, ion exchange chromatography, and gel filtration, or affinity chromatography have been used in isolation and purification [15,35- 37]. The former methods depend on physicochemical properties of proteins while affinity chromatography depends on specific interactions between lectins and a carbohydrate attached to an inert matrix. Although affinity chromatography is a highly specific procedure, some carbohydrate matrices used for affinity chromatography can adsorb not only the lectin but also glycosidases capable of hydrolyzing the sugar structures to which the lectin may bind. Contamination by glycosidases could greatly affect the activity of a lectin preparation [31].

The comparison of the chromatographic pattern of patients with malignant kidney tumors, benign kidney tumors, and non tumoral kidney diseases as well as the healthy individuals exhibits that GalBL could be isolated and purified successfully from sera of patients with malignant kidney tumors, and malignancy of kidney is associated with overexpression of GalBL.

Many laboratories have made considerable efforts to identify a ‘poor prognosis signature’ of tumor- and metastasis-associated genes and to predict the clinical outcome of neoplastic disease. Changes in glycosylation have been shown to strongly associate with the development of cancer and metastasis.

This differential glycosylation of cancerous and healthy tissues is often restricted to altered glycan expression of tumor cells or their secreted glycoproteins [38,39]. In many cases, the structural changes have been further correlated with changes in the activity of one or more glycosyltransferases during the process of transformation from normal to tumor cells. Changes in glycosylation could result in loss of cell adhesion, an event associated with increased cell invasiveness of primary tumors to distant sites [39,40].

Analysis of Serum Crude and Purified Lectins of Patients with Tumoral and Non Tumoral Kidney Diseases and Healthy Individuals: Crude and purified serum proteins were analyzed by polyacrylamide gel and stained with Periodic acid and Silver stains. Periodic acid stain of crude pooled sera of patients and the control group revealed qualitatively incompatible electrophoretic pattern in particular for patients with malignant tumors (figure 4).

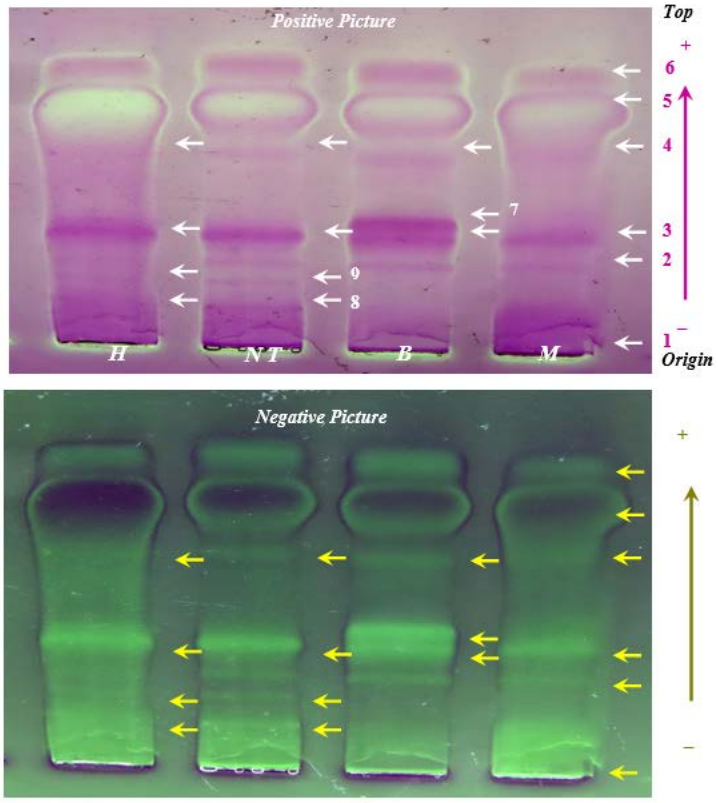

Figure 4: Electrogram of Glycoproteins profile using Conventional Polyacrylamide Gel Electrophoresis (PAGE) 7.5%. Tris - glycin buffer (0.075 M, pH 8.9) was used as the electrode buffer. Prelctrophoresis conditions were 50 mA as a constant current for 30 minutes, with voltage of 15 v/cm, and at 4 ºC. Electrophoresis was carried out for10 minutes at 20 mA. The process was continued for 3.5 hours at 4 ºC by using 40 mA as a constant current and voltage of 15 v/cm. The gel was stained for protein with periodic acid-Schiff. The crude samples that applied were: M: Malignant Kidney Tumors Sera, B: Benign Kidney Tumors Sera, NT: Non Tumoral Kidney Affections Sera, H: Healthy Individuals Sera

The additional bands that appear in glycoprotein profile, particularly in the globulins region due to the changes in cell surface glycoproteins during malignancy, and (or) as a result of synthesis of the acute phase proteins during inflammation processes [40].

Figure 5: Conventional Polyacrylamide Gel Electrophoresis (PAGE) 7.5% for Proteins. Tris - glycin buffer (0.075 M, pH 8.9) used as the electrode buffer. Prelctrophoresis conditions were 50 mA as a constant current for 30 minutes, with voltage of 15 v/cm, and at 4ºC. Electrophoresis was carried out for10 minutes at 20mA, then the process was continued for 3.5 hours at 4ºC by using 40 mA as a constant current and voltage of 15 v/cm. The gel was stained for protein with silver stain. The crude and purified samples that applied were: *Crude Malignant sera sample A: purified GalBL

The approximate molecular weights of purified lectins were determined using conventional PAGE. Five standard proteins with known molecular weighs were used to construct the standard curve as shown in table 5.

Table 5: Standard Proteins Used for the Determination of Purified Lectin Molecular Weights

Standard Proteins	Molecular Weigh (kD)	Number
Lysozyme	13.6	1
Chemotrypsinogene	25	2
Ovalbumin	47	3
Bovine Serum Albumin	67	4
Lactate Dehydrogenase	140	5

The estimated molecular weight of GalBL was 98.40.

The molecular weight of GalBL from calf heart and lung was determined to be approximately 17 kD, and the predominant molecular species had a molecular weight of 9 kD [41]. The molecular weight of the undenatured GalBL purified from human placenta by gel filtration was found to be 26·9 kD. When SDS electrophoresis was applied for this lectin, two subunits with the molecular weight approximate to 13.4 kD for each have been identified [42]. The native molecular mass of galactose binding lectin from seeds of Erythrina speciosa detected by hydrodynamic light scattering was 58 kD and when examined by mass spectroscopy and SDS–PAGE was found to be composed of two identical subunits of molecular mass of

27.6 kD [43]. The purified GalBL from the Latex of Synadenium carinatum lectin appeared to be a glycoprotein with apparent molecular weight of 120 - 130 kD made up of polypeptide chains of 28 and 30 kD [44]. In another study, GalBL purified from pinto beans with a molecular mass of this homodimeric lectin of 62 kD and that of each of its subunits was 31 kD [45].

Characterization of Purified Lectins: To examine the sensitivity of purified lectins in the agglutination reactions, blood of various groups were included in the experiment. Purified GalBL from sera of patients with malignant tumor kidney from sera of patients with malignant kidney tumors was showed its ability to agglutinate RBCs, and the highest agglutination activity was recorded with A^+ blood group. These findings could be explained by differences in glycosylation of the surface proteins of red blood cells [46].

The hemagglutination process was carried out for the purified GalBL in the presence of EDTA. GalBL did not lost the hemagglutination activity, even at concentration of 9 mM of EDTA (which was recorded as the highest concentration of EDTA to complete the inhibition of lectin hemagglutination to crude sera of human lectins). This result clearly indicate that Ca^{2+} is not crucial for the expression of the hemagglutination activity of this lectin, thus; GalBL should be classified as independent calcium lectin type.

The effect of pH on the activity of the purified lectin was investigated. Figure 6 points out that maximal lectin activity was achieved at pH 7.4, while the purified lectin was sensitive to acidic (pH 3) and to basic (pH 12) conditions, under which the activities were completely lost.

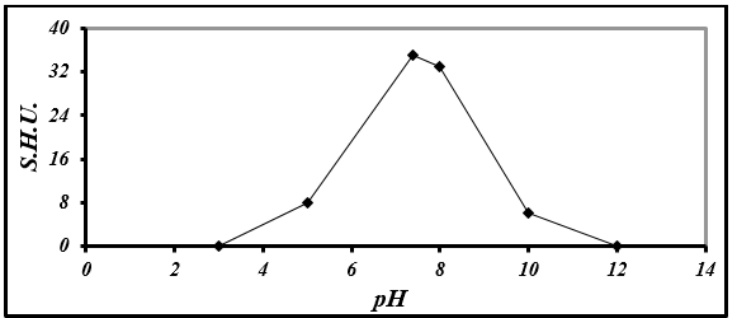

Figure 6: Effect of pH on Purified GalBL Hemagglutination Activity

The conformational change of purified lectin may occur by weakening hydrogen bonds between water and polar groups. Alternatively, the excessive pH may directly affect the interaction between amino acid residues within the protein monomer and facilitate conformational change upon the binding of specific carbohydrates, leading to hydrophobic interaction between the lectin molecules. Moreover, changes in the surface hydrophobicity of the purified lectins may be one of the possible factors affecting the increased irreversible binding to the erythrocyte membrane. According to that, the close relationship between the hydrophobicity enhancement and the oligomerization of purified lectins upon the binding of carbohydrates. Therefore, it seems reasonable to suppose that the hydrophobicity enhancement and the oligomerization of purified lectin reflect structural changes of the purified lectin, which occur during interaction with the erythrocyte membrane.

To explore the effect of temperature on the hemagglutination activity of purified lectin, it was incubated at various temperatures (0°C, 30°C, 40°C, 50°C, 60°C, 80°C, and 100°C) for 1 hour; the mixtures were

cooled until room temperature. The hemagglutination activity was carried out at 30°C (as a optimum temperature to crude lectin hemagglutination). Thermal denaturation results revealed that purified lectin remained stable below 40ºC for 1 hour with no loss of hemagglutination activity, while; it loss about 40% of its hemagglutination activity at 50 ºC. Lectin activity disappeared when the denaturation was carried out at more than 60 ºC (figure 7).

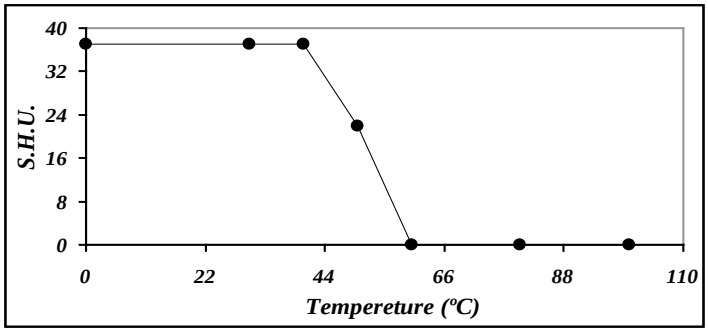

Figure 7: Thermal denaturation of Purified Lectin Hemagglutination Activity

Both 30 and 37 ˚C seem to be more suitable among the examined temperatures for the agglutination process of purified GalBL.

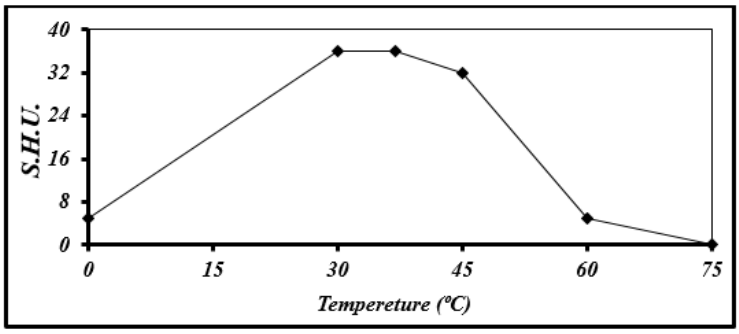

Figure 8: Temperature Effect on the Purified GalBL Hemagglutination Activity

The gradual increase in the purified lectins activity, when the agglutination reaction temperature rises until it reaches its optimum temperature, may be due to the elevation of the kinetic energy for the electrons that leads to weakening or disruption of bonds among the chains of purified lectins, which increase the collision between the interacting molecules, while the observed decrease in this activity when the temperature is more than 37 ˚C may be due to the denature of the protein molecules.

Total carbohydrate contents were estimated by phenol-sulphuric acid method [32] with D-glucose as standard sugar. Carbohydrate was found to compose about 10.8% of GalBL. The results of present study was near to other studies that isolated GalBL from different species [43,47-49].

REFERENCES

[1] Franz H. [1988]: *The ricin story.* Adv. Lectin Res. Vol. 1, p 10-25.

[2] Lis H & Sharon N. [1987]: *Lectins as molecules and as tools.* Ann. Rev. Biochem. Vol. 55, p 35-67.

[3] Jordan E T & Goldstein I J. [1995]: *Site-directed mutagenesis studies on the lima bean lectin.* Eur. Biochem J. Vol. 230, p 958-964.

[4] Sharon N & Lis H. [2004]: *History of lectins: from hemagglutinins to biological recognition molecules.* Glycobiology J. Vol. 14, No. 11, p 53-62.

[5] Hatakeyama T, Unno H, KouzumaY, Uchida T, Eto S, Hidemura H, Kato N, Yonekura M, & Kusunoki M. [2007]: *C-type Lectin-like Carbohydrate Recognition of the Hemolytic Lectin CEL-III Containing Ricin-type-Trefoil Folds.* Biological Chemistry J. Vol. 282, No. 52, p 37826-37835.

[6] Kilpatrick D C. [2002]: *Animal lectins: a historical introduction and overview.* Biochemica et biophysica Acta J. Vol. 1572, No. 2, p 187-197.

[7] Houzelstein D, Gonc¸alves I R, Fadden A J, Sidhu S S, Cooper D N, Drickamer K, Leffler H, & Poirier F. [2004]: *Phylogenetic Analysis of the Vertebrate Galectin Family.* Mol. Biol. Evol. Vol. 21, No. 7, p1177-1187.

[8] Naird D G, Fry B G, Alewood P, Kumar P P, & Kini R M. [2007]: *Antimicrobial activity of omwaprin, a new member of the waprin family of snake venom proteins*. Biochem. J. Vol. 402, p 93-104.

[9] Wong J H, Wong C C, & Ng T B. [2006]: *Purification and characterization of a galactose-specific lectin with mitogenic activity from pinto beans.* Biochemica et Biophysica Acta J. Vol. 1760, p 808-813.

[10] Chandra N R, Kumar N, Jeyakani J, Singh D D, Sharan B. Gowda S B & M. N. Prathima. [2006]: *Lectin db: a plant lectin database*. Glycobiology J. Vol. 16, No. 10, p 938-946.

[11] Jasim R H.[2009]:*Isolation, Purification, and Partial Characterization of Human Lectints from Patients of Kidney Tumors.* Baghdad University, College of Science for Women, Chemistry Department. Treatise.

[12] Pierini C. [2007]: *Lectins: Their Damaging Role in Intestinal Health, Rheumatoid Arthritis and Weight Loss*. Vitamin Research News J. Vol. 21, No. 1, p 1-4.

[13] Abd Alla M D, White G L, Rogers T B, Cary M E, Carey D W, & Ravdin J I. [2007]: *Adherence-Inhibitory Intestinal Immunoglobulin A Antibody Response in Baboons Elicited by Use of a Synthetic Intranasal Lectin-Based Amebiasis Subunit Vaccine*. Infection and Immunity J. Vol. 75, No. 8, p 3812-3822.

[14] Luckenbach J A, Iliev D B, Goetz F W, & Swanson P. [2008]: *Identification of differentially expressed ovarian genes during primary and early secondary oocyte growth in coho salmon, Oncorhynchus kisutch.* Reproductive Biology and Endocrinology. Vol. 6, No. 2, p 1-15.

[15] Ma Y, Cheng W, Gong F, Ma A, Yu Q, Zhang J, Hu C, Chen X, & Zhang D. [2008]: *Active Chinese mistletoe lectin-55 enhances colon cancer surveillance through regulating innate and adaptive immune responses* Gastroenterol. World J. Vol. 14, No. 34, p 5274-5281.

[16] Demers M, Biron-Pain K, Hebert J, Lamarre A, Magnaldo T, & St-Pierre Y. [2007]: *Galectin-7 in Lymphoma: Elevated Expression in Human Lymphoid Malignancies and Decreased Lymphoma Dissemination by Antisense Strategies in Experimental Model.* Cancer Res. Vol. 67, No. 6, p 2824-2829.

[17] Yamamoto H , Nishi N, Shoji H, Itoh A, Hirashima M, & T. Nakamura. [2008]: *Induction of Cell Adhesion by Galectin-8 and its Target Molecules in Jurkat T-Cells.* Biochem. J. Vol. 143, No. 3, p 311-324.

[18] van Till O J W, Modderman P W, de Boer M, Hart H L, Beld Marcel G H, & Boermeester1 M A. [2008]: *Mannose-Binding Lectin Deficiency Facilitates Abdominal Candida Infections in Patients with Secondary Peritonitis.* Clin. Vaccine Immunol. J. Vol. 15, No. 1, p 65-70.

[19] Roos A, Daha M R, Pelt J, & Berger S P. [2007]: *Mannose-binding lectin and the kidney.* Nephrol Dial Transplant. Vol. 22, p3370-3377.

[20] Dhuna V, Bains J S, Kamboj S S, Shanmugavel S J, & Saxena A K. [2005]: *Purification and Characterization of a Lectin from Arisaema tortuosum Schott having in-vitro Anticancer Activity against Human Cancer Cell Lines.* Biochemistry and Molecular Biology J. Vol. 38, No. 5, p. 526-532.

[21] Cookson M S & Chang S S. [2007]: *Malignant Tumors of the Urogenital Tract.* In: *Rakel: Conn's Current Therapy*. 59th Edition. W B Saunders

[22] Miyata Y, Iwata T, Ohba K, Kanda S , Nishikido M, & Kanetake H. [2006]: *Expression of Matrix Metalloproteinase-7 on Cancer Cells and Tissue Endothelial Cells in Renal Cell Carcinoma: Prognostic Implications and Clinical Significance for Invasion and Metastasis.* Clin Cancer Res. Vol. 12, No. 23, p 6998-7003.

[23] Togashi A, Katagiri T, Ashida S, Fujioka T, Maruyama O, Wakumoto Y, Sakamoto Y, Fujime M, Kawchi Y, Shuin T, & Nakamura Y. [2005]: *Hypoxia-Inducible Protein 2 (HIG2), a Novel Diagnostic Marker for Renal Cell Carcinoma and Potential Target for Molecular Therapy.* Cancer Res. J. Vol. 65, No. 11, p 4817-4826.

[24] Eisenberger C F, Schoenberg M, Enger C, Hortopan S, Shah S, Chow N H, Marshall F F, & Sidransky D. [1999]: *Diagnosis of Renal Cancer by Molecular Urinalysis.* Journal of the National Cancer Institute, Vol. 91, No. 23, p 2028-2032.

[25] Han W K, Alinani A, Wu C L, Michaelson D, Loda M, McGovern F J, Thadhani R, and Joseph V. Bonventre J V. [2005]: *Human Kidney Injury Molecule-1 Is a Tissue and Urinary Tumor Marker of Renal Cell Carcinoma.*J Am Soc Nephrol. Vol. 16, p 1126-1134.

[26] Alamdari F I. [2007]: *Renal Cell Carcinoma: Factors of importance for follow-up and survival.* Sweden, Umeå, Umeå University, Urology and Andrology, Departments of Surgical and Perioperative Sciences, New Series, N1138. Thesis.

[27] Perez-Valdivieso J R, Bes-Rastrollo M, Monedero P, de Irala J, & Lavilla F J. [2007]: *Prognosis and serum creatinine levels in acute renal failure at the time of nephrology consultation: an observational cohort study*. BMC Nephrology. Vol. 8, No. 14, p 1-9.

[28] Coutinho E L, Luciana Andrade L N, Chammas, Morganti L, Nestor Schor N, & Bellini M H. [2007]: *Anti-tumor effect of endostatin mediated by retroviral gene transfer in mice bearing renal cell carcinoma.* The FASEB J. Vol. 21, p 3153 – 3161.

[29] Lam J S, Belldegrun A S, & Figlin R A. [2004]: *Tissue Array-Based Predictions of Pathobiology, Prognosis, and Response to Treatment for Renal Cell Carcinoma Therapy.* Clinical Cancer Research. Vol. 10, p 6304s–6309s.

[30] Bradford M. [1976]: *A rapid and sensitive method for the quantitation of microgram quantities of proteins utilizing the principle of protein-dye binding.* Anal. Biochem. J. Vol. 72, p 248-254.

[31] Hermanson G T, Mallia A K, & Smith P K. [1992]: *Immobilized Affinity Ligand Techniques.* UK. Academic Press, Inc.

[32] Dubois M, Gilles K A, Hamilton J K, Robers P A and Smith, F. [1956]: *Colorimetric method for determination of sugars, and related substances.* Annal. Biochem. Vol. 28, No. 3, p350-356.

[33] Iurisci I, Tinari N, Natoli C, Angelucci D, Cianchetti E, & Iacobelli S. [2000]: *Concentrations of Galectin-3 in the Sera of Normal Controls and Cancer Patients.* Clinical Cancer Research. Vol. 6, p 1389-1393.

[34] Algaba F. [2008]: *Renal Adenomas: Pathological Differential Diagnosis with Malignant Tumors.* Advances in Urology. Vol. 2008, p 1-4.

[35] Indravathamma P & Seshadri H S. [1980]: *Lectin from rice*. Biosci. J. Vol. 2, No. 1, p 29-36.

[36] Denis M, Palatty M, Bai N R, & Suriya S J. [2003]: *Purification and characterization of a sialic acid specific lectin from the hemolymph of the freshwater crab Paratelphusa jacquemontii.* Eur. Biochem. J. Vol. 270, p 4348-4355.

[37] Bulgakov A A, Eliseikina M G, Petrova IY, Nazarenko E L, Kovalchuk S N, Kozhemyako V B, & Rasskazov V A. [2007]: *Molecular and biological characterization of a mannan-binding lectin from the holothurian Apostichopus japonicus.* Glycobiology. Vol. 17, No. 12, p1284-1298.

[38] Murray P & Hall J. [2000]: *Renal Replacement Therapy for Acute Renal Failure.* Am. J. Vol. 162, p 777-781.

[39] Raymond R W. [2007]: *Biochemistry of Cancer*. In: *Cancer Biology.* Section 1.p 108-120.

[40] Cho W, Jung K, & Adamec J. [2008]: *Glycoproteins Associated With Breast Cancer.* Abstract from the 4th Annual USHUPO Conference, Bethesda, MD.

[41] De Waard A, Hickman S, & Kornfeld S. [1976]: *Isolation and Properties of P Galactoside Binding Lectins of Calf Heart and Lung.* The Journal of Biological Chemistry. Vol. 251, No. 23, p 7581-7587.

[42] Nambiar M P, Basu D, & Appukuttan P S. [1987]: *Physicochemical properties and binding-site amino acid residues of galactoside-binding protein of human placenta.* Biosci. J. Vol. 11, No. 1, p. 331-338·

[43] Konozy E H, Bernardes E S, Rosa C, Faca V, Greene L J, & Ward R J. [2003]: *Isolation, purification, and physicochemical characterization of a D-galactose-binding lectin from seeds of Erythrina speciosa.* Archives of Biochemistry and Biophysics. Vol. 410, p 222-229.

[44] Souza M A, Amâncio-Pereira F, Ribeiro C, da Silva A G, Silva E G Andrade L R, Deolina J, Lanza H, & Afonso-Cardoso S R. [2005]: *Isolation and Partial Characterization of a D-Galactose-Binding Lectin from the Latex of Synadenium carinatum.* Brazilian Archives of Biology and Technology. Vol. 48, No. 5, p 705-716.

[45] Wong J H, Wong C C, & Ng T B. [2006]: *Purification and characterization of a galactose-specific lectin with mitogenic activity from pinto beans.* Biochemica et Biophysica Acta J. Vol. 1760, p 808-813.

[46] Voet D, Voet J G, Pratt C W. [2006]: *Fundamentals of biochemistry: life at the molecular.*2nd Edition. John Wiley and Sons Inc.

[47] Barbieri L, Falasca A, F ranceschi C, Federico Licastro F, RossiC A, & Stirpe F. [1983]: *Purification and properties of two lectins from the latex of the euphorbiaceous plants Hura*

crepitans L. (sand-box tree) and Euphorbia characias L. (Mediterranean spurge). Biochem. J. Vol. 215, p 433-439.

[48] Hamazak H. [1986]: *Purification and Characterization of aH uman Lectin Specific for Penultimate Galactose Residues.* The Journal of Biological Chemistry. Vol. 261, p 5455-5459.

[49] Melo F R, Benevides N M, Bereira M G, Holanda M L, Meneds F N, Olivera S R, Freitas A L, & Silva L M. [2004]: *Purification and partial characterization of a lectin from the red marine alga Vidalia obtusiloba C Agardh.* Revista Brasil. Bot. Vol. 27, No. 2, p 263-269.

SOCIETY FOR SCIENCE AND EDUCATION UNITED KINGDOM

JBEMi JOURNAL OF BIOMEDICAL ENGINEERING AND MEDICAL IMAGING

ISSN: 2055-1266
VOLUME 2 ISSUE 1

Automated Drusen Detection Technique for Age-Related Macular Degeneration

[1]Kajal Kumari and [2]Deepti Mittal
Electrical and Instrumentation Engineering Department, Thapar University, Patiala (Punjab), India;
[1]Kajalkumari0503@gmail.com; [2]deepti.mittal@thapar.edu

ABSTRACT

Age-related macular degeneration is one of the leading cause of vision loss and blindness among people of age 50 and higher. Macular degeneration is usually characterized by drusen. Drusens are accumulation of lipids, fatty proteins that appears as abnormal white-yellow deposits on the retina. Detection of these lesions using conventional image analysis methods is quite complicated and time taking mainly due to non-uniform illumination and the variability of the pigmentation of the background tissues. This paper presents an automated technique for segmentation and quantitative analysis of drusen in publicly available retinal images i.e. Structured Analysis of retina (STARE) and Automated Retinal Image Analysis (ARIA), acquired with the aid of a digital fundus camera. The present methodology emphasizes on quantitative analysis of drusen based on: First, region-based statistical analysis which corrects the non-uniform illumination of background, enhances local intensity, minimizes image noise, segment image through Otsu's threshold in addition with morphological operation and hence compute area and edge of the detected drusen. Second, pixel-wise feature extraction which extracts the feature of overlapped components through weighted centroid and standard deviation, makes counting of number of drusen easy. Hence, this system can provide vital information about the quantity of drusen and can aid clinicians in their diagnosis to evaluate the stage of age-related macular degeneration.

Keywords: Age-related macular degeneration, non-uniform illumination correction, image denoising, morphological operation, area based analysis, region based properties, fundus images.

1 Introduction

Age-related macular degeneration (AMD) is a common eye condition, main cause of irreversible blindness in the developed countries and a third main cause of blindness in the whole world [1]. It is characterized by drusen or yellow pigmentation. Drusen is basically accumulation of fatty deposits, lipids and waste material from different layers of the retina. AMD is classified into two types: wet and dry. Dry, or atrophic, macular degeneration are characterized by drusen and wet or exudative macular degeneration are also known as late AMD. About 10 percent of people who have macular degeneration have the wet form which will deteriorate the macula i.e. central vision [2]. Currently, no treatment exists for late AMD. However, early detection and quantitative mapping of retinal abnormalities can provide timely treatment and also the progression of disease may be slow down. Number and area of drusen are used to grade AMD [3]. Manual calculation of drusen is time consuming, labor-intensive, difficult to

DOI: 10.14738/jbemi.21.913
Publication Date: 24th February 2015
URL: http://dx.doi.org/10.14738/jbemi. 21.913

reproduce and may lose important information. Thus there are various methods have been used to detect drusen automatically or semi-automatically based on thresholding [4, 5], feed forward neural network [6, 7], template matching [8], spatial histogram [9], drusen modelling [8] and Hybrid classifier [10, 11]. However, none of these methods have achieved accurate result in counting exact number of drusen. An alternative method based on region based statistical properties has been implemented to improve the identification of exact number of drusen by decomposing the overlapped components through their weighted centroids.

This paper present an automated retinal fundus drusen detection system with an ultimate goal being to automatically assess the risk for development of AMD. First, it plays an important role for reliably localize drusen against the varying lesions present in background. Second, to correct the non-uniform illumination due to uneven surface of retina. Third, it improves image noise, count total no. of drusen, its area and edge. In this paper edge of the drusen is detected by canny edge detector. It is widely used in computer vision to locate sharp intensity changes and to find object boundaries in an image which makes edge of the drusen sharp.

2 Materials and method

Materials

2.1 Retinal fundus imaging:

Two publicly available datasets i.e. STARE and ARIA are used to test the performance of applied drusen detection method. The STARE dataset consists of 36 normal and 47 AMD images acquired with TOPCON fundus camera with 35 degree field of view and a resolution of 700 x 650 pixels. The ARIA dataset consists of 101 normal and 60 AMD images acquired with Carl Zeiss Meditec camera with 50 degree field of view and a resolution of 768 x 576 pixels [16, 17].

Method

2.2 Region based statistical analysis

As illustrated in Figure 2, the integrated image analytics of applied system consists of several image processing procedures. These include retinal fundus image as an input. In order to detect drusen, green channel is selected because it having better contrast than other channels, correction of non-uniform illumination by creating an approximation of the background through morphological opening and then subtract this approximated image from original image, enhancement of image is done by automatic contrast enhancement, segmentation of image is done by Otsu's threshold, noise is removed by morphological operation. A label matrix is created after segmentation to visualize the drusen as a pseudo color indexed image. Decomposition of overlapped components in an image is obtained by calculating the object properties which is based on pixel-wise feature extraction through weighted centroid of mass. Weighted centroid is also used to locate the exact the position of spot that has been blurred over an image region by the image acquisition process. Edge of the drusen is detected by canny edge detector which classifies a pixel as an edge if the gradient magnitude of the pixel is larger than those of pixels at both its sides in the direction of maximum intensity change.

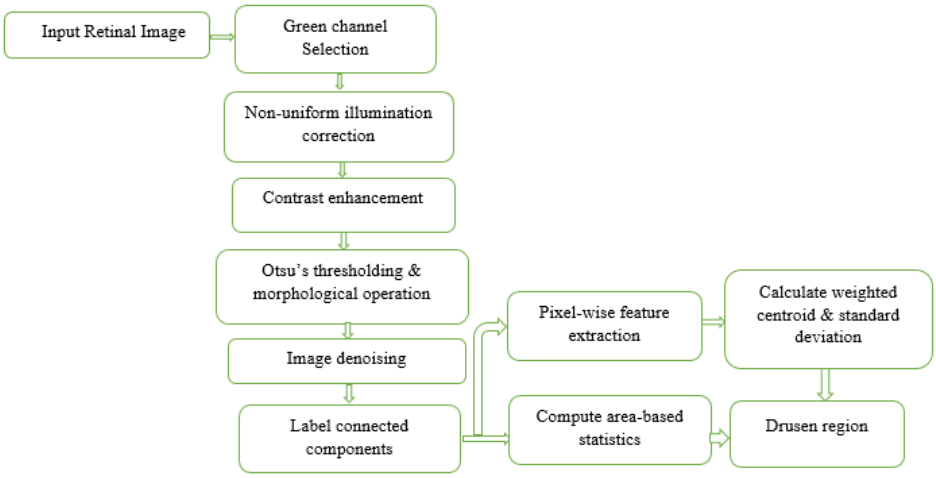

Figure 1: Flow chart of proposed automated drusen detection system

2.2.1 Selection

Green channel is selected from color retinal fundus images because it gives better contrast which helps in extracting brightest region from the background [12].

2.2.2 Non-uniform illumination correction

Retinal images having non-uniform illumination because these are acquired with digital fundus camera, which captures the illumination reflected from the retinal surface. There are also several other factors like curved surface of retina, pupil dilation, cataract & unexpected movement causes severe distortions in the resulting image.

Background of an image having non-uniform illumination hence to make background illumination more uniform, create an approximation of the background as a separate image by removing all the foreground using morphological opening. When this approximate image view as a surface it shows the variation of illumination. Now subtract this approximated image from the original image which will give a uniform image. Morphology is a tool for extracting image components that are useful in representation and description of region shape [13]. The opening operation has the effect of removing objects that cannot completely contain the structuring element, in this erosion is followed by dilation [14].

$$Dilation, (I_m \oplus S_t)(x,y) = \max_{i,j}[I_m(x-i, y-j) + S_t(i,j)] \quad (1)$$

$$\text{Erosion}, (I_m \ominus S_t)(x,y) = \min_{i,j}[I_m(x+i, y+j) - S_t(i,j)] \quad (2)$$

$$Opening, \quad I_i \circ S_t = (I_m \ominus S_t) \oplus S_t \quad (3)$$

Where I_m is image on which we have to do the operation & S_t is the structuring element. I_i is the resultant image after opening operation. (x, y) is the co-ordinate of an image and (i, j) is the coordinate of structuring element.

2.2.3 Contrast Enhancement

Necessity of contrast enhancement arises due to non-ideal acquisition during imaging hence Automatic contrast enhancement is used. It is a technique for mapping an image's intensity value to a new range. In this technique the values in the intensity image $g(x, y)$ is transforms to values in $f(x, y)$ by mapping values between low and high to the values between bottom and top

[1]. The values below low and above high are clipped i.e. values below low map to bottom and those above high map to top.

2.2.4 Drusen detection

To efficiently detect drusen, a combination of mathematical morphology and Otsu's algorithm is used. Binarization of the retinal image is done by using Otsu's algorithm [15], to separate complex regions from the smooth ones. This technique partition the image into two classes $w_0 = \{0,1,2, \dots t\}$ and $w_i = \{t+1, t+2, \dots L-1\}$ at a gray level t, where L represents the total no. of gray levels of the image. Let n_i be the number of pixels at ith gray level, and the total no. of pixels in a given image be n. the probability of occurrence of gray level i is defined as $P_i = n_i/n$. The probabilities of the two classes w_0 and w_i are $q_1(t)$ and $q_2(t)$ are calculated, as shown in Eq. (4)

$$q_1(t) = \sum_{i=0}^{t} p_i \ , q_2(t) = \sum_{i=i+1}^{L-1} p_i \tag{4}$$

The mean of the classes are then computed as

$$\mu_j(t) = \sum_{i=0}^{t} iP_i/q_j(t) \tag{5}$$

Let σ_B^2 and σ_T^2be the between-class variance and total variance respectively. An optimal threshold t^* can be obtained by maximizing the between-class variance as given in Eq. (6).

$$t^* = Arg\left\{\max_{0 \le i \le L-1} (\sigma_B^2/\sigma_T^2)\right\} \tag{6}$$

After applying segmentation the largest connected region is marked as a candidate for drusen. The image obtained after segmentation having objects which can be referenced separately as shown in Eq. (7). Otsu's global thresholding technique has been used to make the proposed system robust and prevents the user intervention during the execution.

$$I_i(r,c) = \begin{cases} 1, & if\ I(r,c) \in object\ labeled\ 'i' \\ 0 & otherwise \end{cases} \tag{7}$$
$$where, r \in [0 \dots Height-1] and\ c \in [0 \dots Width-1]$$

Background noise will be removed through mathematical morphology as given in Eq. (1) and (2). Mathematical morphology also helps to remove the irrelevant vessels from the drusen region. A structuring element is used by selecting the size and shape of the neighborhood. In an image to add the pixels to the boundaries, dilation is used and to remove the pixels from the boundary erosion is used.

The shape and size of the structuring element determines the number of pixels added or removed from the image. After detecting drusen a label matrix is created to display it as a pseudo colour indexed image. Pseudo colour is used to compute total no. of drusen present in an image and then find area of each object through Eq. (8).

$$\text{Area,} \qquad A_i = \sum_{r=0}^{H-1} \sum_{c=0}^{W-1} I_i\,(r,c) \tag{8}$$

The area A_i is measured in pixels and it indicates the relative size of the object.

2.2.5 Pixel-wise feature extraction

In this step object properties is calculated by weighted centroid using pixel value of gray scale image. The (gray value weighted) center of mass is often useful to locate the exact position of a spot that has been 'blurred' over an image region by the image acquisition process. This will also help in decomposition of overlapped objects into individual particle. Hence exact number of drusen can be evaluated by an Eq. (9) and (10).

$$\bar{r_i} = \frac{1}{A_i} \sum_{r=0}^{H-1} \sum_{c=0}^{W-1} r I_i\,(r,c) \tag{9}$$

$$\bar{c_i} = \frac{1}{A_i} \sum_{r=0}^{H-1} \sum_{c=0}^{W-1} c I_i(r,c) \tag{10}$$

The Eq. (9) and (10) corresponds to the row and column where the centre of mass is located. This attribute will help to locate the objects in a bi-dimensional image.

$$f(x,y) = \sqrt{\frac{1}{mn-1} \sum_{(r,c)\in w} [g(r,c) - \frac{1}{mn-1} \sum_{(r,c)\in w} g(r,c)]^2} \tag{11}$$

Eq. (11) is used to calculate standard deviation. It is used for custom calculation based on pixel values of the original grey scale image. The 'pixel values' property returns a vector containing the greyscale values of pixels in a region. Where, $f(x,y)$ is the grey image on which standard deviation is represented. $g(r,c)$ is the binary image on which standard deviation is calculated, mn represents the size of the image.

Conventional edge detector is used to find the edge of the drusen which is basically canny edge detector.

3 Results and Discussion

This algorithm is tested on 36 images, publically available datasets i.e. STARE and ARIA, acquired by the Fundus camera. It is observed from the Figure 2 that the green channel is selected for further processing because it having better contrast than the other channels.

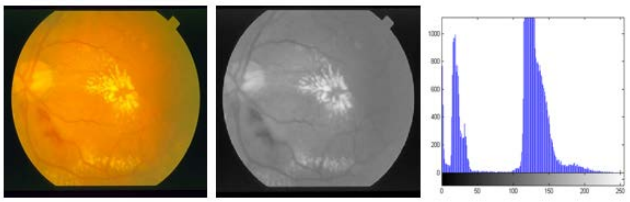

Figure 2: Green channel selection, (a) color retinal fundus image from STARE dataset, (b) green Channel of fundus image, (c) histogram of green channel having better contrast.

Central part of the retina is focused by defining a rectangle at the right or left side of the optical nerve (right or left eye, respectively). Figure 3. Presents example of gray-scale version (green band) of the original color image. Drusen show up as bright blobs, but automatic extraction of these pathological features is difficult, since drusen vary in shape and size and tend to spread (varying brightness) around their location. Additionally, small bright regions of the background tend to create larger than can be mistaken as large drusen hence to remove such type of false negative, an approximation of background as a separate image is considered by using morphological operation. A surface plot of background is shown in Figure 3 to visualize the variation of background. After subtracting this approximated image from the original image a uniform image is obtained which shows the variation in drusen and background.

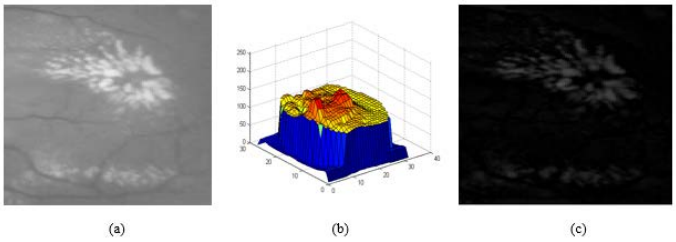

Figure 3: Result of non-uniform illumination and contrast enhancement, (d) test image from Original gray image, (e) surface plot of approximated background, (f) image with uniform illumination after subtracting approximated image from original image

Contrast of an image has been enhanced by using automated contrast enhancement technique which enhanced the local intensity globally. Segmentation of an image is done by Otsu' threshold which ideally locate candidate region of drusen and with the help of morphological operation noise can be removed. There is no vague results found. Pseudo color indexed image is used for visualization of no. of drusen present in retinal fundus images as shown in Figure 4.

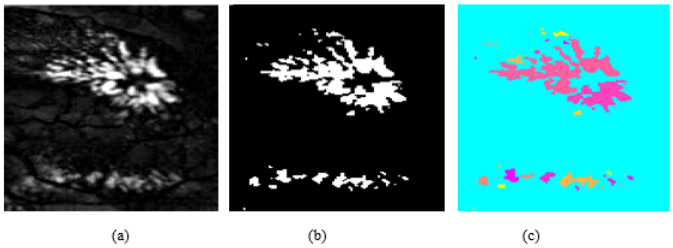

Figure 4: Result of segmentation, (a) enhanced image, (b) binarization of image using Otsu's thresholding (c) Pseudo color indexed image

Pixel-wise feature extraction is done in binarized image to identify the total number of drusen present in image. As drusen varies in its shape and size which may be overlapped on each other. Therefore pixel-wise feature extraction is used because which is based on calculation of weighted centroid and standard deviation of individual pixels. As in Figure 5. Weighted centroid and standard deviation of individual components can be visualize by above mentioned Eq. (10, 11). Graph shows the regional maximum intensity with respect to standard deviation which shows the intensity of individual components.

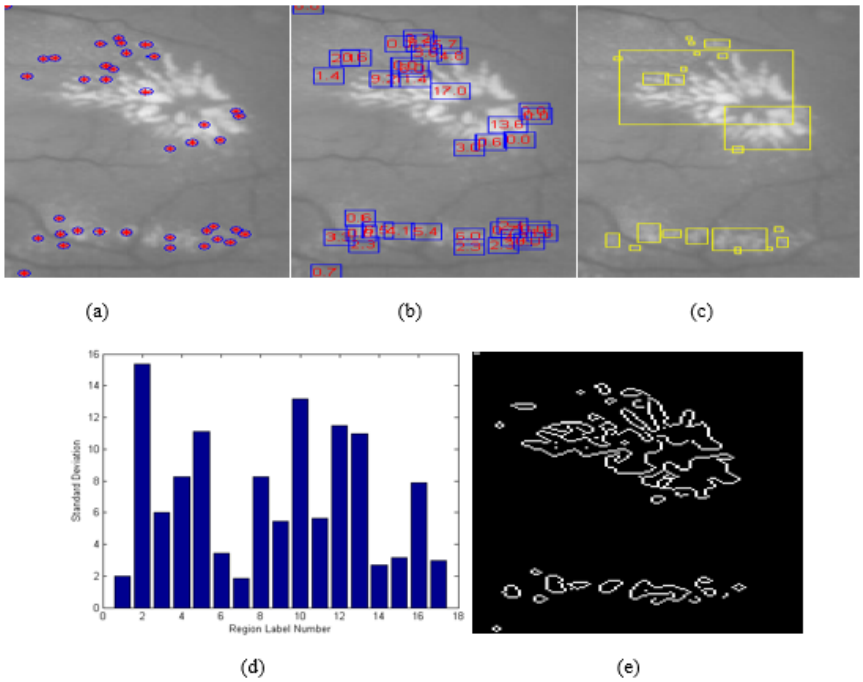

Figure 5: Results of drusen detection, (a) weighted centroid of components, (b) standard deviation of objects in image, (c) components with standard deviation>2, (d) regional label no. w.r.t standard deviation, (e) edge of drusen through conventional edge detector.

Canny edge detector is used to detect the edge of each individual drusen. The canny edge detector is widely used to locate the sharp intensity changes and to find object boundaries in an image. It classifies a pixel as an edge if the gradient of the pixel is larger than those of pixels at both its sides in the direction of maximum intensity change. Area is calculated by an Eq. (8) in pixels. The total area affected by drusen is in pixels. The proposed algorithm has been tested on an image as shown in Figure 5. (e) Which shows the edge of the drusen and its total area in pixels is 1698 pixel.

4 Conclusion

Early detection of drusen may reduce the progression of disease and also provide timely treatment. In this work, an automated detection of drusen using publicly available retinal fundus images is proposed. It analyzes region and custom properties of image by extracting the feature from the pixels of fundus images. This algorithm will help in computing the total area affected by drusen in pixels with its edge. Centre of mass (weighted centroid) with standard deviation is used to separate out different objects which helps in calculating total number of drusen present in image. Use of the proposed detector may reduce false negatives and give reliable results in both area and number of drusen.

REFERENCES

[1] Resnikoff, Pascolini, et al. Global data on visual impairment in the year 2002. Bulletin of the World Health Organization, vol. 82, 2004. p: 844-851.

[2] De Jong, Age-related macular degeneration. The New England Journal of Medicine, 355(14), 2006. p: 1474-1485.

[3] Age-related Eye Disease Study Research Group, The age-related eye disease study system for classifying age-related macular degeneration from stereoscopic color fundus photographs: the age-related eye disease study report number 6. American Journal of Ophthalmology, vol. 132, 2001. p: 668-681.

[4] Smith, Chan, et al. A method of drusen measurement based on reconstruction of fundus background reflectance. Br J Ophthalmol, 2005. 89: p: 87-91.

[5] Rapantzikos, M. Zervakis, et al. Detection and segmentation of drusen deposits on human retina: Potential in the diagnosis of age-related macular degeneration. Medical image Analysis 7, 2003. p: 95-108.

[6] Thaibaoui, Raji, et al. A Fuzzy Approach to Drusen Detection in Retinal Angiographic Images. IEEE, 2000. p: 748-751.

[7] Checco, Corinto, Cnn-based algorithm for drusen identification. 2006 IEEE International Symposium on Circuits and Systems, 2006. p: 2181-2184.

[8] Mora et al. Automated drusen detection in retinal images using analytical modelling algorithms. Biomedical Engineering Online, 2011. p: 10:59.

[9] Lee, Smith, et al. Learning Non-Homogenous Textures and the Unlearning Problems with Application to Drusen Detection in Retinal Images. IEEE, 2008. p: 1215-1218.

[10] Zheng, Vanderbeek, et al. An Automated Drusen Detection System for Classifying Age-Related Macular Degeneration with Color Fundus Photographs. IEEE 10th International Symposium on Biomedical Imaging, 2013. p: 1448-1451.

[11] Raza, Rafique, et al. Hybrid Classifier Based Drusen Detection in Colored Fundus Images. IEEE Jordan Conference on Applied Electrical Engineering and Computing Technologies, 2013. p: 8-13.

[12] Rama Prasath, M.M.Ramaya, Automatic Detection and Elimination of an Optic Disc for Improving Drusen Detection Accuracy. Fifth International Conference on Signal and Image Processing, 2014. p: 117-121.

[13] Gonzalez, R. and R. Gonzalez, R. and R. Woods (2007). Digital Image Processing – third addition, Prentice-Wall.

[14] Gupta, Purkayashta, Statistical Particle Analysis in Microscopic Images using Morphology. International Journal of Science and Advance Technology, 2012. Vol. 1, No. 1, p: 35-40.

[15] N Otsu, A threshold selection method from gray-level histogram, IEEE transection on systems, Man and Cybernetics, SMC-8, 1978, p: 62-66.

[16] ARIA database from http://www.eyecharity.com/aria_online .

[17] STARE database from http://www.ces.clemson.edu/~ahoover/stare .

[18] D. Jayanthi, Devi, et al. Automatic diagnosis of retinal diseases from color retinal images. International journal of computer science and Information Security, 2010. Vol. 7, No. 1

[19] Parvathi, N. Devi, Automatic drusen detection from color retinal images. IEEE International Conference on computational Intelligence and Multimedia Applications, 2007. p: 377-381.

[20] Kanagasingam, Bhuiyan, et al. Progress on Retinal image analysis for age related macular degeneration. Progress in Retinal and Eye Research 38, 2014. p: 20-42.

[21] Mookiah K., Achrya, et al. Automated diagnosis of Age-related Macular Degeneration using greyscale features from digital fundus images. Computers in Biology and Medicine 53, 2014. p: 55-64.

SOCIETY FOR SCIENCE AND EDUCATION
UNITED KINGDOM

JBEMi JOURNAL OF BIOMEDICAL ENGINEERING AND MEDICAL IMAGING

ISSN: 2055-1266
VOLUME 2 ISSUE 1

Segmentation and Measurement of Exudates in Fundus Images of the Retina for Detection of Retinal Disease

[1]Jaskirat Kaur and [2]Deepti Mittal
[1]Department of Electronics and Communication Engineering,
Chandigarh College of Engineering and Technology, Panjab University, Chandigarh, India;
[2]Department of Electrical and Instrumentation Engineering,
Thapar University, Patiala, India;
[1]Jaskiratkaur17@gmail.com; [2]deeptimit@gmail.com

ABSTRACT

Retinal diseases are asymptomatic in nature with the significant effect of vision loss. With the growing number of retinopathy cases each year there is a requirement of the evaluation of large amount of database. This has led to the development of numerous automated and semi-automated evaluation methods to track the retinal diseases. In this study, a simpler automated method is developed to diagnose retinal disease as far as exudates are concerned. Previously used segmentation methods do not generate very satisfactory results mainly because the composition of exudates which are degenerated regions in retinal fundus image is non homogeneous. Therefore an alternative method for segmentation is developed to use the homogeneity of healthy regions than degenerated regions. The developed technique initially separates the healthy regions like blood vessels and optic disc from the retinal fundus images and classifies as healthy. Further the dynamic region growing method is employed for the segmentation of exudates in the images containing diabetic retinal disease. The technique developed is examined on various retinal images and the outcomes reveal that the presented technique performs better than the previous proposed methods for the segmentation of exudates.

Keywords: Retinal Fundus Images; Optic Disc; Blood Vessels; Automated Segmentation of Exudates.

1 Introduction

One of the most significant complications causing severe damages to the retina is retinopathy. Subsequently it causes visual loss and blindness in some cases if medical treatment is not given on time. Diabetic retinopathy is diagnosed by structural alterations in the retina, which can be exploited in the image processing for the automated detection and diagnosis of disease. As the disease develops over a period of time, continuous monitoring is necessary to diagnose the early symptoms so that timely effective treatment can be taken [1-3]. Manual segmentation of retinal images is quite difficult and the clinician may make mistakes during the process [3,5]. Also this is a very time consuming process. Therefore an automated system for the segmentation of disease could diminish the workload of the experts. The degenerations in retinal fundus images are segmented and then the disease can be measured by the system. After the automatic segmentation of lesion if further analysis is required it is

DOI: 10.14738/jbemi.21.987
Publication Date: 24th February 2015
URL: http://dx.doi.org/10.14738/jbemi. 21.987

examined by the expert. Grade of the segmentation carried out is determined by the type and quality of the acquired image, experience and expertise of the clinician.

Recent studies have shown that retinal diseases like diabetic retinopathy can be analyzed from fundus images of the retina [4,6,10]. Segmentation and measurement of the development of different degenerations associated with this disease like microaneurysms (MA), Cotton wool spots (CWS), hard exudates (HE) etc. is quite difficult due to their irregular structural variations. Currently numerous semi-automated and automated methods are being used for the lesions segmentation associated with retinal diseases.

Automated assessment of pathologies related to retina requires the accurate segmentation landmarks such as of optic disc and blood vessels from the retinal fundus image, so that lesions can be extracted from the image successfully. Gracia et al. proposed a radial basis function classifier to detect HE and also various other features were extracted from retinal fundus image [14]. The section which suitably distinguished exudates and background of the retinal fundus image was chosen by applying logistic regression method prior to the application of normalization and segmentation of candidate areas. Post-processing techniques are applied on the retinal fundus images to eliminate the noisy regions. Other studies employ preprocessing methods like shade correction, normalization and image enhancement on retinal fundus images. Further they apply diameter closing and an automatic threshold scheme for detection of candidate portions which are categorized as unhealthy and healthy [11].

Degenerations associated with retinal diseases are non-uniform and intricate in shapes. Thus, efficient segmentation of these ill shaped structures requires complicated and expensive methods. On the contrary, healthy compositions of retinal fundus images have uniform shapes, and segmentation of these uniform shapes is much easier as compared to the non-uniform shapes. In the previous studies, numerous techniques have been proposed for the precise segmentation of lesions associated with retinal fundus images but are not very effective in proper and accurate segmentation of various retinal pathological regions because of the irregular and non-uniform patterns and complex structures of the lesions. In this study, a converse technique is developed for segmentation and quantification of exudates. This method is simple as compared to earlier methods as it utilizes the background retinal image for measuring exudates for the detection of retinal disease. The developed method is quite efficient, less expensive and promising as compared to the earlier techniques developed.

The paper is structured as follows. A brief of the previous segmentation techniques in literature for detecting various lesions in retinal fundus images are presented in Section 2. A brief outline of techniques used in the segmentation such as location of optic disc, determining background image and elimination of blood vessels are presented in Section 3. Section 3 also explains the dynamic region growing and threshold based technique with background image for segmentation of exudates associated with retinal disease. Performance estimation measures are explained in Section 4. The results of performance measures are presented and discussed in Section 5. The conclusions and future work are presented in Section 6.

2 Background

With the idea of researchers designing automated system for detection of retinal disease numerous techniques in literature exist for the segmentation of exudates, location of optic disc, segmentation and elimination of blood vessels to screen and monitor retinal disease in retinal fundus images [8,13,18]. Most of previous segmentation methods developed are dependent on matched filters, image thresholding, edge detection, matched filters and tracking models [9,15,22]. Pattern recognition method, automatic model based detection, texture analysis, and mathematical morphology based methods have also been proposed for the detection of degenerations in retinal images. Few of these methods work on location and detection of landmark structures in retinal fundus images [19,23]. These methods mainly concentrate on segmentation and detection of only one type of landmark structure like blood vessels or optic disc [23–25]. Also few techniques detect more than one features and lesions in retinal fundus images [1,22,28]. Sinthanayothin et al. employed a multi-layer perceptron neural net in which inputs are acquired from a principal component analysis method for edge detection in retinal fundus images for optic disc detection [29]. Various techniques are also presented in literature for detection of optic disc, fovea and other landmark structures in retinal fundus images [19,23]. In addition, Walter et al., Quellec et al., Xu et al., established automated techniques for detection of MA's [11,16,30].

Numerous other approaches were presented for automatic segmentation of degenerations associated with retinal disease [8,12,15]. Even though number of techniques has been developed in this domain, those are restricted by one or other following limitations. At the initial step, clinician is required to determine the region of interest and the techniques were also not entirely automated. Differing image conditions may produce imperfect and unacceptable kinds of segmentations. Also, most of the earlier segmentation techniques if applied to detect one type of lesion it overlaps with other degenerations related to retinal diseases. Lastly, various segmentation algorithms in proposed methods need huge computational efforts and time.

3 Methods Used in the Segmentation of Exudates

Number of methods has been employed for the automatic segmentation of diabetic retinopathy such as vessel elimination methods, background image extraction method and Optic disc detection methods. In such methods, firstly images are transformed into 2^8 levels gray value retinal fundus images and background image of healthy portions is separated from the converted gray value retinal fundus image.

Our method first generates the background reference image as shown in figure1.

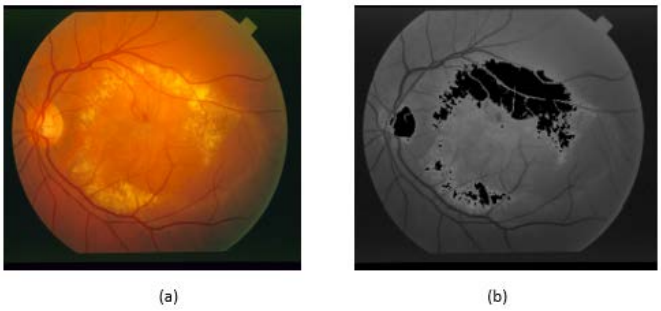

Figure 1: (a) Original Image (b) Reference Background Image

After the segmentation of retinal fundus image optic disc detection is carried out for location and elimination of optic disc region. To discard the blood vessel shapes from the resulting segmented retinal fundus image vessel elimination method is applied.

Retinal image is thus divided based on low and high intensity regions and the dynamic threshold value is used to segment the intensity with higher value and high contrast lesions in the retinal fundus image. So, the clear and bright regions are separated by the means of dynamic thresholding and converse segmentation method. This method uses dynamic thresholding method and conforms itself to intensity variations across the entire retinal fundus image and produces better results than the earlier methods used in the literature. First the method segments the healthy structures in the image and then conversely segments unhealthy portions from the retinal fundus images. The flow diagram of the above processes is shown in figure 2.

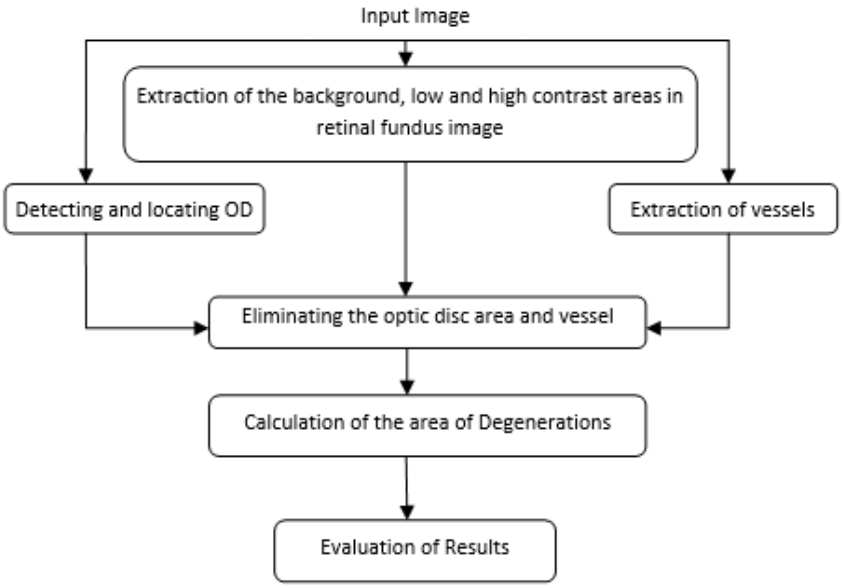

Figure 2: The Flow Diagram of the Algorithm Proposed

Steps in the automatic segmentation technique for detecting exudates are as the following:

- Extraction of the reference background image of healthy regions in the retinal fundus image.
- Identification and segmentation of high and low contrast areas in the image.
- Location and detection of optic disc.
- Extraction of vessels
- Elimination of vessels and optic disc region.
- Calculation of the area of anatomic structures and lesions in the image.
- Generating statistical parameters to objectively evaluate the algorithm.

3.1 Steps for Locating and Eliminating the Optic Disc

Optic disc is one of anatomical structures in retinal images. Thus the location and detection of optic disc is crucial in analysis and quantification procedure of degenerations in retinal fundus images. The distinct

properties of optic disc like high intensity; circular geometric structure etc. can be utilized in the detection. In the literature, various methods are used to segment [13,32] and detect [19,23,26] optic disc in retinal images. In this method transformed sobel filter given by Equation (1), it makes edges in the image clearer.

$$\mathrm{Img}_{\mathrm{fil(i,j)}} = \frac{\sum_{k=1}^{n} \mathrm{abs[img\_ver\_fil(i+k,j)]+abs[img\_hori\_fil(i,j+k)]}}{n} \quad (1)$$

Where k stands for the distance shown in figure 3., (i, j) depicts the value for current pixel and $\mathrm{Img\_fil}(i, j)$ represents the filtered image. $\mathrm{img\_ver\_fil}[(i + k, j)]$ and $\mathrm{abs[img\_hori\_fil}(i, j + k)]$ represent vertical and horizontal sobel operations.

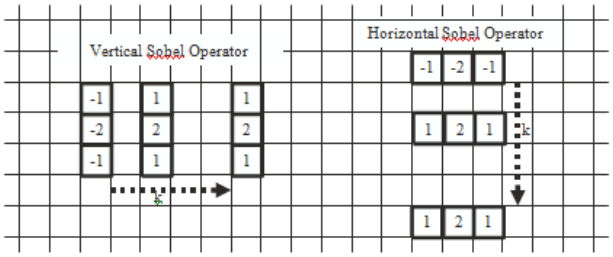

Figure 3: Transformed vertical and horizontal sobel filters

In the given Equation (1), to obtain the blood vessel boundaries clearly in the resultant image n is set to 3 so that edges of the optic disc could be applied to detect the position of optic disc. In order to utilize the distinctive features of the vessels in the optic disc region the histogram of the processed image is computed and the extreme values of the horizontal and vertical histogram of the processed image around optic disc are identified to detect the optic disc. The blue lines on the figure 4 around the optic disc determine the location of optic disc.

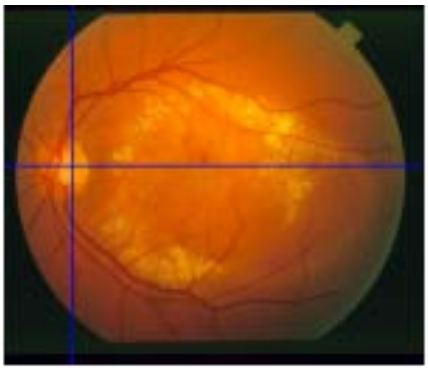

Figure 4: Identification of location of optic disc

The image is processed using transformed sobel filter and high contrast regions are determined using the reference background image. Then these high contrast regions are eliminated from the processed image by examining the region surrounding the present pixel value. If the eighty percent of the region around optic disc shows high intensity values, the pixels are discarded. Small fragments of the vessel and noisy parts are also discarded from the filtered image.

Optic disc region may also be detected as retinal degeneration portions and thus degenerations cannot be measured correctly. Therefore optic disc region must be discarded from the resulting segmented image. Pixels around the optic disc are discarded by taking the average diameter of the optic disc.

3.2 Elimination of Blood Vessels in Retinal Images

A large number of techniques are presented in literature for detection and segmentation of vessels in fundus images [9,21,24,27]. Retinal images consist of a large variety of vessel structures and these should be discarded properly to enhance the precision of the resulting segmented image containing exudates.

The intensity value of each pixel is examined and if it is found within the required interval with respect to the reference background image, it is taken as the blood vessel and taken as the healthy portion or else classified as unhealthy. The interval changes dynamically according to the reference background image. Consequently, all blood vessel shapes are eliminated for segmenting exudates successfully. Vessels are segmented using the method proposed by Kose et al. [31].

3.3 Modified Dynamic Region Growing Technique with Reference Image

Degenerations due to retinal disease may occur over the entire retinal fundus image and the average intensity may vary across the whole retinal fundus image. The segmentation method should tolerate these changes to segment the images efficiently. The difference of the reference image and the average of the pixels segmented is successfully measured by applying Equation (2).

$$\mathrm{Img(i,j)\_seg} = (\text{Healthy if } \left|\mathrm{Img_{org(i,j)}} - \mu + \alpha_{l,u}\left[\mathrm{Img_{bgnd(i,j)}} - \mu\right] - \beta\left[\mu - \mathrm{Img_{org(i,j)}}\right]\right| \leq \Delta,$$
$$\text{unhealthy if otherwise or vessel} \quad (2)$$

Where

- $\mathrm{Img(i,j)\_seg}$ are the segmentation results,
- $\mathrm{Img\_org(i,j)}$ depicts the intensity value of the present pixel,
- μ represents the average value of the segmented pixels,
- Δ Represent the reference threshold value which is approximately adjusted to 8.8.
- β Represent average value correction constant, which is approximately adjusted to 0.49.
- $\mathrm{Img\_bgnd(i,j)}$ is the background image and α is the background toleration constant.

$$\left|\mathrm{Img\_org(i,j)} - \mu + \alpha_{l,u}[\mathrm{Img\_bgnd(i,j)} - \mu] - \beta[\mu - \mathrm{Img\_org(i,j)}]\right| \leq \Delta \text{ is used as}$$
$$-\Delta + \mu - \alpha_l\,[\mathrm{Img\_bgnd(i,j)} - \mu] < Img\_org(i,j) < \Delta + \mu - \alpha_u\,[\mathrm{Img\_bgnd(i,j)} - \mu] \quad (3)$$

Thus $\alpha_{l,u}$ contain maximum and minimum cut of values which are constants and the values are set experimentally to 0.93 and 0.49.

Thus intensity variations over the entire retinal image are measured and degenerations across the retinal fundus image are segmented efficiently. Modified dynamic region growing technique used adjusts by its very nature to the varying intensity conditions and efficiently segment exudates over the whole retinal fundus image without needing any requirement of the clinician. One of the tested

segmented images is shown in figure 5. Dynamic region growing method achieves best segmentation performance as far as previous region growing methods are concerned.

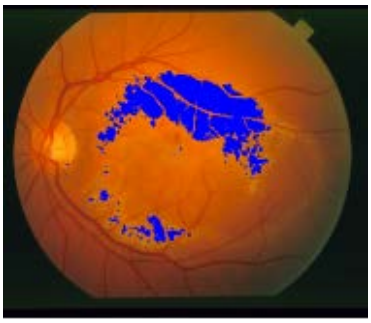

Figure 5: Final Segmented image containing exudates

3.4 Segmentation Method for Detecting Dark Lesions

The approach is to segment the region with lower intensity value as compared to the background image intensity value. Thus the low intensity regions consist of blood vessels and low contrast degenerations. Further the segmentation of vessel technique utilized in [29] is applied to eliminate the vessels. The areas which are left prior to the segmentation of vessels are the low contrast degenerations and considered as the unhealthy portion of the retinal image. Threshold constant is adjusted just below the intensity value of the reference background image. Therefore the pixels whose intensity value is lower than the above adjusted threshold constant is categorized unhealthy portion prior to the elimination of vessels. These pixels are set to blue in the resulting image.

4 Performance Evaluation Measures Used

In the medical field, the eye specialists have to handle huge amount of retinal fundus images. Therefore, an automated segmentation and quantification technique may facilitate the experts to analyze the images more speedily. The presented technique automatically segments exudates in retinal fundus images found in the progression of retinal disease.

As mentioned earlier, experiments prove that manually segmenting and measuring retinal degenerations are somewhat complex and difficult, and the clinician may simply make faults during the process of segmentation [1–3]. Nature of segmentation carried out also varies based on the quality of the retinal fundus image and knowledge of the clinician. In this proposed approach, three performance measures are used to obtain the effectiveness of segmentation method used.

Tp - true positive, Tn - true negative, Fn - false negative and Fp - false positive.

Sensitivity and specificity are also mainly used mathematical performance measures to present the results in more comprehensible form. Sensitivity is the fraction of true positives rightly categorized by the technique. Specificity is the fraction of the true negatives rightly categorized by the technique. Sensitivity and specificity measures are computed by applying Equation (4) and (5).

$$\text{Sensitivity} = \frac{\text{Tp}}{\text{Tp+Fn}} \tag{4}$$

$$\text{Specificity} = \frac{\text{Tn}}{\text{Tn+Fp}} \tag{5}$$

In this proposed application, a simpler technique is used to determine the area and magnitude of retinal degenerations based on Equation (6).

$$\text{Deg\_area} = \sum_{i=1}^{M} \sum_{j=1}^{N} \{\text{Pixel}(i,j)\} . \text{seg} \quad (6)$$

Where Deg_area is the degenerated area in the retina. Pixel(i,j) Represent the pixels in the region as unhealthy portion, is adjusted to 1, and seg represents segmentation outcomes. In this method, seg is set to 1 for pixels which are already segmented and 0 for other remaining pixels.

5 Results

In the study carried out, a total of 128 retinal fundus images with 760 × 570 pixels resolution in various varieties as shown in Table 1 were utilized to estimate the effectiveness of the method presented. The retinal images were acquired from digital retinal fundus camera in SGHS hospital located in Sohana, Punjab, India. A number of the retinal fundus images, including 57 images with apparent optic disc, were also utilized to test optic disc location and identification performance of the system. Figure 5 shows the tested retinal fundus image with HE and its automatic segmentation results.

To present the variations in the segmentation of retinal disease, distributions of the degenerated portions in retinal images are shown in Table1. It is observed that most of the retinal degenerations are distributed over the entire retinal fundus image.

Table 1: Distributions of Hard Exudates in Retinal Fundus Images.

Distributions of HE in Retinal Images	No. of Images	In percent
HE spread around Macula	38	29.68
HE spread around whole image	90	70.3
Total no. of Images	128	100

In order to evaluate the efficiency of the method proposed, developed system is tested on retinal fundus images with varying sizes of HE namely small, medium and large. The basic step in our method is to locate the position and detect the optic disc in numerous types of cases. Thus, the developed database for measuring the performance of the system in optic disc localization and detection comprises of all types of retinal fundus images. On the contrary, images with retinal disease are utilized for the quantification of the HE segmentation performance.

In the optic disk identification and location, mainly the outcomes are obtained for the retinal images with the retinal disease. Results for identification of optic disc and elimination of optic disc region are given in Table 2. The results depict about on an average 96.1% of the optic disc on the images with varying sizes of degeneration, are identified efficiently.

Table 2: Identification and Location of optic disc (OD)

OD No. of Images	Identification and Location of OD		
	Precisely	Roughly	Wrongly
57 Images with clear OD	42	13	2
71 Images with non-clear OD	54	14	3
Total %age	96.1% Located correctly		

To evaluate the performance of the segmentation technique used for hard exudates sensitivity and specificity parameters are measured, and their results are shown in Table 3. In all tests carried out all over the paper, the threshold constant was kept same and parameters mentioned above are used to generate consistent and comparable results. Therefore, minute under and over segmentations are seen in few of the test cases. However the developed technique is still very promising in detection and segmentation of HE.

Table 3: Performance Measures for the Detection of Hard Exudates.

	Hard Exudates	
	Sensitivity	**Specificity**
Images with small lesions	0.981	0.986
Images with medium lesions	0.972	0.998
Images with large lesions	0.984	0.998
Average	0.979	0.994

In the previous work, numerous techniques are implemented for segmentation of retinal disease in retinal fundus images [2,13,15,22,29]. The evaluation of the technique on the database images with hard exudates is about 98.65% which is better than the previous techniques proposed in the literature. The results in Table 3 show that the modified dynamic region growing technique provides a superior performance among other segmentation techniques mentioned in the study.

6 Conclusion

In the literature several techniques produce various performance parameters in the segmentation of degenerations associated with retinal disease and optic disc detection. The methods employed with expert requirement produce approximately 91% of segmentation precision [2,7,8,15,17]. On the contrary, OD localization performance parameter values of these techniques are also around 95% [20,26]

In order to segment exudates dynamic region growing method is used. The developed technique, tested on 128 retinal fundus images, showed higher precision in segmentation than the other techniques. The entire interpretation of a particular retinal fundus image was carried out in around 7 seconds without any expert involvement. The method locates and detects approximately 96.1% of the ODs and segments approximately 98.65% of exudates precisely. Thus, the technique provides a better segmentation and quantification precision. Also the complexity, cost and time of the system is reduced at the much comparable results. The proposed method also has the ability to eliminate blood vessels in the retinal fundus images, and it also discards the optic disc region to quantify exudates area precisely.

The method proposed for segmentation of exudates can also be utilized for analyzing and segmentation of other types of retinal lesions in retinal fundus images, which could be taken as a subsequent work. There exist some cases in which image illumination artifacts come in account in retinal fundus images where the proposed technique is not able to attain good segmentation performance. In other methods proposed the image illumination artifacts may influence the segmentation performance adversely, which could also be taken as additional problem of subsequent tasks to be solved.

REFERENCES

[1] M. Wilson, P. Soliz, S.C. Nemeth, *Computer-aided methods for quantitative assessment of longitudinal changes in retinal images resenting with maculopathy*. Medical Imaging, 2002. 4681: p. 150-170.

[2] C.I. Sanchez, R. Hornero, M.I. Lopez, J. Poza, *Retinal image analysis to detect and quantify lesions associated with diabetic retinopathy.* Engineering in medicine and Biology Society, IEMBS. 26th Annual International Conference of the IEEE, 2004: p. 1624-1627.

[3] T. Smith, V. Sivagnanavel, J.K. Chan, et al., *An inter-institutional comparative study of drusen segmentation and quantification using a digital technique of fundus background reconstruction*. Investigative Ophthalmology & Visual Science, 2004. 45.

[4] K. Rapantzikos, M. Zervakis, K. Balas, *Detection and segmentation of drusen deposits on human retina: potential in the diagnosis of age-related macular degeneration*, Medical Image Analysis, 2003: p. 95-108.

[5] T.J. Wolfensberger, P.A.M. Hamilton, *Diabetic retinopathy- an historical review.* Royal Swets & Zeitlinger. Seminar in Ophthalmology, 2001. 16: p.2-7.

[6] R.T. Smith, J.K. Chan, T. Nagasaki, et al., *Automated detection of macular drusen using geometric background leveling and threshold selection,* Archives of Ophthalmology, 2005. 23: p.200-206.

[7] Walter, J.C. Klein, P. Massin, A. Erginay, *A contribution of image processing to the diagnosis of diabetic retinopathy - detection of exudates in color fundus images of the human retina*, IEEE Transactions on Medical Imaging, 2002. 21: p.1236-1243.

[8] A. Sopharak, B. Uyyanonvara, S. Barman, et al., *Automatic detection of diabetic retinopathy exudates from non-dilated retinal images using mathematical morphology methods.* Computerized Medical Imaging and Graphics, 2009. 32: p.720-727.

[9] A.W. Reza, C. Eswaran, S. Hati, *Diabetic retinopathy: a quad tree based blood vessel detection algorithm using RGB components in fundus images.* Journal of medical systems, 2008. 32: p.147-155.

[10] M. Niemeijer, B. van Ginneken, S.R. Russell, et al., *Automated detection and differentiation of drusen, exudates, and cotton-wool spots in digital color fundus photographs for diabetic retinopathy diagnosis*. Investigative ophthalmology & Visual Science, 2007. 48: p. 2260-2267.

[11] T. Walter, P. Massin, A. Erginay, R. Ordonez, C. Jeulin, J.-C. Klein, *Automatic detection of microaneurysms in color fundus images.* Medical Image Analysis, 2007. 112: p. 555-566.

[12] K. Estabridis, R.J.P. de Figueiredo, *Automatic detection and diagnosis of diabetic retinopathy* ICIP. IEEE International Conference, 2007.2: p.445-448.

[13] S.S. Lee, M. Rajeswari, D. Ramachandram, B. Shaharuddin, *Screening of diabetic retinopathy-automatic segmentation of optic disc in colour fundus.* Proceedings of DFMA. The 2nd International Conference on Distributed Frameworks for Multimedia Applications, 2006: p. 37-43.

[14] M. García, C.I. Sánchez, J. Poza, M.I. López, R. Hornero, *Detection of hard exudates in retinal images using a radial basis function classifier.* Annals of Biomedical Engineering. Springer,2009.37: p. 1448-1463.

[15] S.S. Basha, K.S. Prasad, *Automatic detection of hard exudates in diabetic retinopathy in diabetic retinopathy using morphological segmentation and fuzzy logic.* IJCSNS. International Journal of Computer Science and Network Security, 2008. 8: p. 211-218.

[16] G. Quellec, M. Lamard, P.M. Josselin, G. Cazugel, B. Cochener, C. Roux, *Optimal wavelet transform for the detection of micraaneurysms in retina photographs.* IEEE Transactions on Medical Imaging, 2008. 27: p.1230-1241.

[17] C. Agurto, V. Murray, E. Barriga, et al., *Multiscale AM-FM methods for diabetic retinopathy lesion detection.* IEEE Transactions on Medical Imaging, 2010. 29: p. 502-512.

[18] D. Satyarthi, B.A.N. Raju, S. Dandapat, *Detection of diabetic retinopathy in fundus images vector quantization technique.* Annual India Conference. IEEE INDICON, 2006: p. 1-4.

[19] C. Sinthanayothin, J.F. Boyce, H.L. Cook, T.H. Williamson, *Automated location of the optic disc, foves, and retinal blood vessels from digital color fundus images.* British Journal of Ophthalmology, 1999. 83: p.902-910.

[20] H. Li, O. Chutatape, *Automatic location of optic disc in retinal images*. Proc. IEEE-ICIP 2, 2001: p. 837-840.

[21] O. Chutatape, L. Zheng, S.M. Krishnan, *Retinal blood vessel detection and tracking by matched Gaussian and kalman filters. A tutorial review*. Proc. 20th IEEE Conf. on Engineering in Medicine and Biology Society, 1998: p. 3144-3149.

[22] H. Narasimha-Iyer, A. Can, B. Roysam, C.V. Stewart, H.L. Tanenbaum, A. Majerovics, H. singh, Robust *detection and classification of longitudinal changes in color retinal fundus images for monitoring diabetic retinopathy.* IEEE Transactions on Biomedical Engineering, 2006. 53: p.1084-1098.

[23] M. Niemeijer, B. Ginneken, F. Haar, *Automatic detection of the optic disc, fovea, and vascular arch in digital color photographs of the retina*. Proceedings of the British Machine Vision Conference, 2005: p. 109-118.

[24] K.A. Vermeer, M. Vos F., H.G. Lemij, et al., *A model based method for retinal blood vessel detection.* Computers in Biology and Medicine, 2004. 34: p. 209-219.

[25] H. Li, W. Hsu, M. Li Lee, Ho. Wang, *A piecewise Gaussian model for profiling and differentiating retina vessels*. Proceedings of ICIP-2003, 2003. 1: p. 69-72.

[26] A. Osareh, M. Mirmehdi, B. Thomas, R. Markham, *Comparison of color spaces for optic disc localization in retinal images*. Proc. 16th IEEE Int. Conf. Pattern Recognition, 2002. 1: p. 743-746.

[27] M. Al-Rawi, M. Qutaishat, M. Arrar, *An improved matched filter for blood vessel detection of digital retinal images*. Computers in Biology and Medicine. 37: p. 262-267.

[28] K. Akita, H.A. Kuga, *Computer method of understanding macular fundus images.* Pattern Recognition, 1982. 15: p.1-443.

[29] C. Sinthanayothin, Vi. Kongbunkiat, S. Phoojaruenchanachai, A. Ingalavanija, *Automated screening system for diabetic retinopathy*. Proc. lSPAO3, 2003: p. 915-920.

[30] J.A. Xu, O. Chutatape, *Auto-adjusted 3-D optic disk viewing from low – resolution stereo fundus image.* Computers in Biology and Medicine, 2006. 36: p. 921-940.

[31] C. Köse, *Fully automatic segmentation of coronary vessel structures in poor quality X-ray angiogram images.* Lecture Notes in Computer Science. LNCS. Springer. 4109: p. 72-82.

[32] M. Niemeijer, M.D. Abramoff, B. van Ginneken, *Segmentation of the optic disc, macula and vascular arch in fundus photographs.* IEE transactions on Biomedical Engineering, 2007. 26: p. 116-127.

SOCIETY FOR SCIENCE AND EDUCATION UNITED KINGDOM

JBEMi JOURNAL OF BIOMEDICAL ENGINEERING AND MEDICAL IMAGING

ISSN: 2055-1266
VOLUME 2 ISSUE 1

A SOS Heart Smart Wrist Watch App for Heart Attack Patients

[1]Iqra Memon, [2]Sehreen Gopang, [3]Sapna Bai and [4]Sasuee Rajper
Institute of Biomedical Engineering & Technology, LUMHS Jamshoro, Pakistan
[1]iqrariazmemon@gmail.com; [2]reen_gopang@yahoo.com [3]sapnabai12bme26@gmail.com;
[4]sasueerajper12bme27@gmail.com;

ABSTRACT

Heart disease is one of the main causes of death around world, claiming approximately 17.3 million lives annually, 43% are of cardiovascular disease. Heart ailment can be drastically curtailed by new innovations like with SOS Heart app patients receive immediate emergency assistance in inaccessible areas by performing CPR (Cardio Pulmonary Resuscitation) & AED (Automated External Defibrillator) and other medications. In Heart attack, proper care in first 2 to 3 hours after an incident can increases the rate of survival. The purpose of this field SOS Heart app is to provide quick assistance to the victim in public places by Smart wrist watch which measures physiological parameters and mobile which connected to smart watch via Bluetooth. [1][15][16]

Key Terms: SOS Heart app, Smart Wrist Watch, Bluetooth, Heart Attack, CPR, AED.

1 Introduction

Cardiovascular disease is one of the leading causes of death all over the world, claiming 17.3 million lives in a year. In United States due to increased ratio of cardiovascular disease people die after every 33 seconds. In Pakistan each year, 200,000 people die only due to cardiovascular disease. Up to 2030 expected cardiovascular deaths rate will be 23 million annually. Every year 7, 85,000 Americans have first coronary heart attack. And by 2020, heart disease will be the leading cause of death throughout the world. [14]

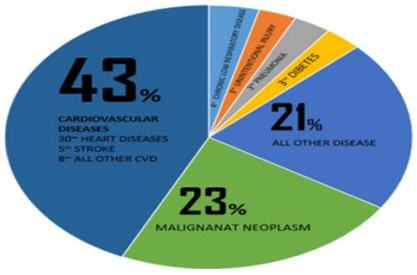

Figure 1: Disease statistics in America

DOI: 10.14738/jbemi.21.981
Publication Date: 26th February 2015
URL: http://dx.doi.org/10.14738/jbemi. 21.981

Mostly Heart Attack occurs at remote areas like shopping malls, on roads etc. where is no medical facility is available. In medical terminology heart attack referred as Acute Myocardial Infarction (AMI). The major cause of Heart Attack is High Blood pressure, hypertension and atherosclerosis (hardening of arteries). When Heart Attack occurs heart stop rhythm, irregular beats are appeared which is also called as arrhythmia (dysrhythmias) and body temperature of victim also varies at that moment. Heart Attack is Coronary Heart Disease (CHD) caused to fatty acid deposition in the inner walls of arteries become narrowing and flow of oxygen-rich blood to section of heart is stopped. So heart is unable to restore normal function and muscles die off, sometimes heart attack symptoms last for 30 minutes or longer. But immediately after Heart Attack first 2 to 3 hours are very important for the survival of the patient. Quick treatment is essential to open blocked arteries and reduces the muscle damage. If quick treatment is not provided to person then chances of death are very high. In remote areas AED, CPR is quick treatment for Heart Attack victims, drugs also used for immediate response to prevent blood clot like Aspirin and other anti plateletes. [17][8]

Yet, there are so many applications available but SOS Heart smart wrist watch app give correct assistance. Artificial intelligence is used which reduce the ratio of mortality due to arrthymias or heart attack. This app is also useful when a person is on a visit to remote areas and heart attack occurs and suffers from Heart Attack complications. Smart wrist watch sends information to mobile via Bluetooth, and mobile sends an emergency text message to health care centre and other saved contacts in this app like family members and doctors. Health care centre automatically trace patient location and reach to rescue that person. This type of app will bring a great impact for CHD patients in the world so they can spend their lives easily without any danger.

2 Procedure

Smart wrist watch SOS heart app intelligence base work deliberately. When a person get heart arrthymias at place where no any emergency health care is available. This app save the life by sensing patient's present physiological condition then collect the data/ Information and send to mobile via Bluetooth. This information is send to persons saved contacts i.e family member, doctor and emergency health care centre through mobile. This app also trace the location of patient and prevent the longer risk of patient critical condition.

Figure 2: SOS Heart App for Heart Attack Patients

3 Methodology

How can the iPhone or mobile detect heart attack? The app works with a sensor connected to smart wrist watch. This smart wrist watch uses low energy 4.0 Bluetooth technology. SOS Heart app can also detect changes in pulse (heart) rate, respiratory rate, body temperature and body movement position in case of patient fells down. If any change detected in parameters, smart watch send a signal to mobile, then mobile will automatically send a message to particular saved contacts in app via text or an emergency alert. In this app patient can save data related to disease which can be very useful for health care professionals in case of he / she may have allergy of any drug.

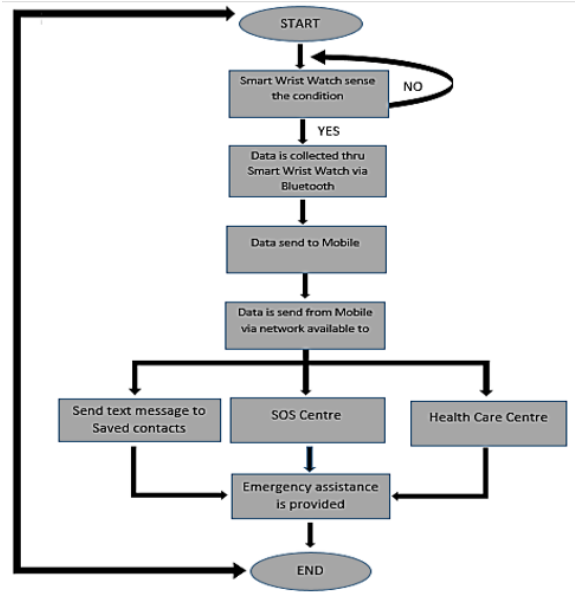

Figure 3: is shown How Chart of Victim Critical Condition occurs and how emergency assistance is provided

4 Sensor Technology

The heart rate monitor includes a Bluetooth technology, which means it requires a Bluetooth 4.0 capable Phone it is difficult on a simple android. It requires a hand set that has a BT 4.0, as well as android 4.3 or higher. This Smart watch runs on a battery cell CR2032 coin. Battery life duration is about 6 to 11 months depending on its usage.

4.1 Supported Sensor

For Smart wrist watch supported sensors are: Nuubo's, nECG, Zephyr's Bio Harness, Smartphone internal sensors (accelerometer, gyroscope, light) Bluetooth and mobile network.

Figure 4: Is showing Smart wrist watch with sensor and SOS app on Mobile

5 Advantages

- SOS Heart smart wrist watch accessory have been designed to benefit peoples in heart attack and other cardiovascular diseases.
- This app gets location of patient and sent a short message alert to patient's contacts and health care center via a text message or calling an emergency number.
- SOS Heart app that allows the user to add vital details like Blood group, medical history and details of patient that can be helpful in an emergency situation. [18]

6 Disadvantages

- SOS Heart app does not send any text if network is not available.
- In some cardiovascular disease symptoms are not appear, so Smart wrist watch does not sense any change and can't send data to mobile.
- SOS Heart smart wrist watch have limited range of Bluetooth.
- Due to improper functioning of Smart wrist watch sensor accuracy will be limited.

7 Conclusion

In order to prevent the person from heart arrhythmias at remote areas. This research is based on emergency SOS Heart app Smart wrist watch. This SOS Heart app provides quick assistance to the victims by Smart wrist watch via Bluetooth, to the mobile. This app will reduce the mortality ratio due to arrhythmias or Heart attack. SOS Heart app also detects changes in pulse rate, respiratory rate, body temperature and body movement positions in case of incidence. This app also allows the user to add vital details and medical history related to patient that can be fruitful in an emergency situation. It is expected through this app in limited time, quality of life can be improved.

REFERENCS

[1] Dr Durairaj Ponraj, Dr Zhiqiang Luo. Field testing of SOSHeart: A mobile app to call for help in Emergency. Journal of Assistive Rehabilitative & therapeutic Technologies 2013, 1:22501.

[2] Shyamal Patel, Hyung Park, Paolo Bonato, Leighton Chan and Mary Rodgers. A review of wearable sensors and systems with application in rehabilitation. J Neuroeng Rehabil. 2012; 9: 21. doi: 10.1186/1743-0003-9-21

[3] Sharon Profis. Do wristband heart trackers actually work? A checkup. @Sharon Profis / May 22, 2014 5:30 AM PDT.

[4] R.Soniyapriyadarshini. Case study on smart wearable sensors and systems with application in rehabilitation. International Journal of Scientific & Engineering Research, Volume 4, Issue 5, May-2013. ISSN 2229-5518.

[5] Tuba Yilmaz, Robert Foster and Yang Hao. Review Detecting Vital Signs with Wearable Wireless Sensors. Sensors 2010, 10, 10837-10862; doi:10.3390/s101210837.

[6] Smartphone mHealth emergency App and device for heart attack prediction and assistance. [By EMResponse] [Powered By NovoED].

[7] Smartphone Apps. http://emergency2.0wiki.org/ . 24 October 2014, at 01:16.

[8] iHELP. www.iHELP emergency care network.html. Copyright © 2014 iHELP World Ltd.

[9] Mary Elizabeth Dallas | Medically reviewed by Farrokh Sohrabi, MD. Having a Heart Attack or Stroke? Your iPhone Knows. 8/30/2013.

[10] Naina Khedekar. Smartphones.5-inch iBall Andi Uddaan with dedicated SOS button launched for Rs 8,999. 17 Dec 2013, 17:46.

[11] Heart Disease: Scope and Impact. http://www.theheartfoundation.org. Copyright©2015 The Heart Foundation.

[12] James Beckerman, MD, FACC. Heart Disease Health Center. http://www.webmd.com . October 03, 2014 © 2014 WebMD, LLC.

[13] Heart Disease Statistics. www.Heart Disease Statistics.mht. Copyright © 2013 American College of Cardiology Foundation.

[14] Muhammad Qasim. International The News. http://www.thenews.com.pk/Todays-News-6-134656-Cardiovascular-diseases-claim-200,000-lives-annually-in-Pakistan . Sept 29, 2012.

[15] Sarah Barbour. Healthy America (Heart Disease). http://healthy-america.blogspot.com/. Jun 28, 2012.

[16] Heart disease Scope and impact. The Heart Foundation. http://www.theheartfoundation.org

[17] Reviewed by Thomas M. Maddox, MD.Heart and cardiovascular disease. http://www.webmd.com/heart-disease/guide/diseases-cardiovascular . June 11, 2012

[18] Emergency panic button alert. https://play.google.com/store/apps/details?id=com.incorporateapps.emergency&hl=en. Oct 24, 2014.

SOCIETY FOR SCIENCE AND EDUCATION UNITED KINGDOM

JBEMi JOURNAL OF BIOMEDICAL ENGINEERING AND MEDICAL IMAGING

ISSN: 2055-1266
VOLUME 2 ISSUE 1

Contrast Enhancement Technique for CT Images

[1]Kanika Sharma and [2]Deepti Mittal
Department of Electrical and Instrumentation Engineering,
Thapar University, Patiala, Punjab, India
[1]kanika.3991@gmail.com; [2]deepti.mittal@thapar.edu

ABSTRACT

The images obtained by computed tomography (CT) scanning are gray scale images, in which gray level shades are almost similar around the tissue. CT images must be enhanced for easy visualization of the lesion or tumor. This paper proposes a contrast enhancement technique for medical CT images, based on modification of histogram equalization technique. Modification is done by adding a constrained variable offset to the transformation function of global histogram equalization. This constrained variable offset helps to preserve the mean brightness of the image, which prevents the global outlook of CT image. Texture of structural part of CT images was enhanced by this algorithm, due to which tumor or infected region is easily visible. The proposed technique was applied on liver CT images containing tumor and its performance was evaluated by subjective evaluation and three quantitative measures.

Keywords: global histogram equalization, constrained variable offset, cumulative distributive function, transformation function.

1 Introduction

Enhancement of computed tomography (CT) medical images is needed to visualize the tumor and disease portion of image correctly and easily. CT images have low contrast in the gray level distribution of tissue part in the image, because of that, small tumors and infected parts are not clearly visible. Texture of the CT images is needed to be improved to visualize the disease, especially small tumors. Texture can be enhanced by enhancing the contrast of the image (without taking background in consideration). The proposed technique helps in enhancement of texture of the CT image so that tumor region is easily visible to the radiologist with less fatigue.

There are many contrast enhancement techniques in literature, global histogram equalization (GHE) is one of the most common techniques, but the main drawback of this technique is artifacts because of over enhancement [1]. The main purpose of this technique is to make uniform histogram distribution of the image. Due to this, histogram of the enhanced image sometimes over stretched and global outlook of image is disturbed, which is not desirable in images. Local histogram equalization (LHE) is extension of histogram equalization (HE) and used to enhance the local details of the image, which GHE fails to do [1,2]. LHE also enhances the noise with the local details. Dynamic histogram equalization (DHE) [3] technique is also based on conventional HE. DHE divides the histogram of image into sub-parts according to the local minima and equalize each part after assigning them specific gray values.

DOI: 10.14738/jbemi.21.914
Publication Date: 26th February 2015
URL: http://dx.doi.org/10.14738/jbemi. 21.914

Constrained variational histogram equalization (CVHE) is a very effective technique used for contrast enhancement with preserving the global appearance of the image [4, 5]. In this technique variational approach of histogram equalization is used with a constraint that preserves the mean brightness. A weighting mean- separated sub- histogram equalization (WMSHE) technique enhances the contrast by separating the histogram of image based on weighting mean function and equalizing each sub part by its small scale value [6]. This technique also preserves the overall luminance of the image. The range limited bi-histogram equalization (RLBHE) technique is also proposed to maintain the global look of the enhanced image by preserving the mean luminance of the image [7]. This technique divides the histogram into two sub parts according to a threshold in order to minimize the intra class variance. Due to this the object is separated from background and contrast is enhanced separately. Contrast limited adaptive histogram equalization (CLAHE) technique enhances the contrast by dividing the image matrix into tiles (blocks), after enhancing the contrast of all tiles separately, it combines the neighboring tiles using bilinear interpolation to avoid the blocking effect [8].

The proposed technique, histogram equalization with constrained variable offset (HECVO) is also based on the histogram equalization. This technique uses the conventional transformation function of HE to enhance the contrast, by adding a variable offset to it, which will preserve the mean brightness of the enhanced image.

2 Global Histogram Equalization Technique

Let hi(r) and ho(s) are the normalized histogram of the input image and output image (enhanced image) respectively, where r and s are the normalized random variables for gray level. A transformation function is used to map the gray level rx of input image to gray level sx of output (enhanced) image [1], where r, s ϵ [0, L]:

$$s = T(r) \tag{1}$$

The transformation function used for image enhancement in GHE is cumulative distribution function (CDF):

$$s = T(r) = \sum_{x=0}^{r} hi(x) \quad \text{for r=0,1....L} \tag{2}$$

For gray scale images (8-bit images) L is equal to 255.

3 Proposed Technique

The proposed technique is histogram equalization with constrained variable offset (HECVO). This technique is divided into two stages:

1. Contrast enhancement using transformation function of global histogram equalization.
2. Preserve the mean brightness of image by adding the constrained variable offset to the transformation function.

In first stage, transformation function of histogram equalization is obtained using CDF, and applied to image to enhance the contrast of the input image. Contrast of the image is enhanced, but the global outlook changes and mean brightness of image is not equal or closer to the original image. Therefore,

the transformation of GHE is taken as the base function of the algorithm and an offset is added to it in second stage.

In second stage, mean brightness of the output or enhanced image is preserved, so the image retains its global outlook. To achieve this objective Δλ constrained variable offset is added to the transformation of HE. This offset is added or subtracted according to the output image brightness, if output image is brighter than the input image then Δλ is subtract acted from the original transformation function and if the output image is darker than the input image then Δλ is added to transformation function in order to make the mean brightness of the output image closer or equal to the input image. When global histogram equalization is applied to the CT images, it produces brighter images than original. It implies that for CT images offset is subtracted from the original transformation function, so new transformation function is:

$$T(r) = \sum_{x=0}^{r} hi(x) - \Delta\lambda \tag{3}$$

Δλ is constrained variable offset, it controls the over stretching produced by the global HE and it varies according to the histogram values of the input image. It is calculated as follows:

$$\Delta\lambda = |k| - \left(\frac{|k|}{L+1} \times x \right) \tag{4}$$

Where x is bin value of gray scale histogram of the input image, k is a constant obtained iteratively according to the mean brightness difference ΔM. k is initiated by any arbitrary value, say k=1, then apply the transformation function in eq.(3) and calculate the mean brightness difference ΔM. Iteratively increase or decrease the value of k (according to the mean brightness of output image) till the mean brightness difference is minimized. Mathematical formula for mean brightness difference is:

$$\Delta M = \frac{\left(\sum_{x=0}^{r} x \times hi(x) - \sum_{x=0}^{r} T(r) \times hi(x) \right)}{m \times n} \tag{5}$$

Where (m×n) is size of the original image.

The transformation function of proposed technique performs controlled stretching of histogram of image for contrast enhancement with global outlook similar to the original image.

4 Performance Evaluation Methods

The proposed algorithm is applied to the liver CT images. The performance evaluation is done subjectively by visual inspection of radiologist and quantitative analysis (objective analysis) is done by calculating three measures: root mean square contrast (RMSC) [9], root mean square error (RMSE) [4], absolute mean brightness error (AMBE) [4].

RMSC is used to measure the contrast value of the image, higher contrast value shows the high contrast enhancement. Mathematical formula for RMSC is:

$$RMSC = \sqrt{\frac{1}{m \times n} \sum_{i=0}^{m-1} \sum_{j=0}^{n-1} \left(I(i,j) - \bar{I} \right)^2} \tag{6}$$

Where ($m \times n$) is the size of the mage, $\bar{I}$ is the average intensity of all pixel values in the image. The image I is assumed to have its pixel intensities normalized in the range [0, 1].

RMSE is used to quantify the distortion or change produced by the enhancement operator. Lower value of RMSE shows low distortion in the image. Increment in contrast value is also considered as distortion, but this distortion is required for enhancement of image. Therefore, distortion is produced with contrast enhancement but this distortion must not so high that image overall appearance changes. Mathematical formula for RMSE:

$$RMSE = \left(\frac{1}{m \times n} \sum_{i=0}^{m-1} \sum_{j=0}^{n-1} \left(I(i,j) - I^*(i,j) \right)^2 \right)^{\frac{1}{2}} \tag{7}$$

Where I and I^* are the original and enhanced images, respectively.

AMBE is defined as the difference between mean brightness of input image and mean brightness of output image. To preserve the global appearance of image, the AMBE value should be low. Mathematical formulas for AMBE:

$$AMBE = \left| \mu_o - \mu_i \right| \tag{8}$$

Where μ_i *and* μ_o are mean brightness of the input and output images, respectively.

5 Results and Discussion

The proposed technique is evaluated both subjectively and quantitatively on a data set containing 75 CT images, out of which some CT images are shown in Fig. 1. Arrows in the images point to the infected portion of tissue. The size of images is 514×514 pixels. The data set of CT images is taken from the MAX hospital, Delhi, India. Processed techniques are implemented in MATLAB version 7.10. Visual inspection of enhanced images shows that the texture of the liver tissues is enhanced and image details are more clear, due to which tumor is easily visible as compared to original image. The enhanced images are assessed and approved by radiologist. The subjective evaluation is supported by three quantitative measures shown in Table 1.

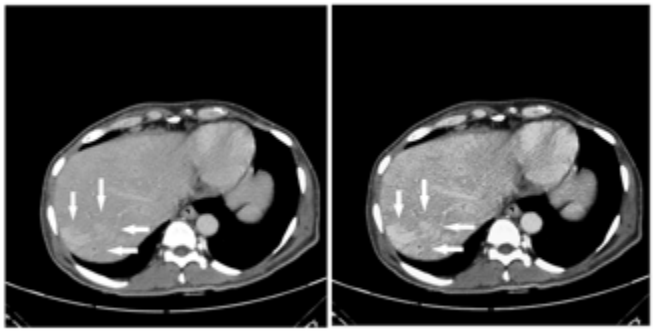

(a) (b)

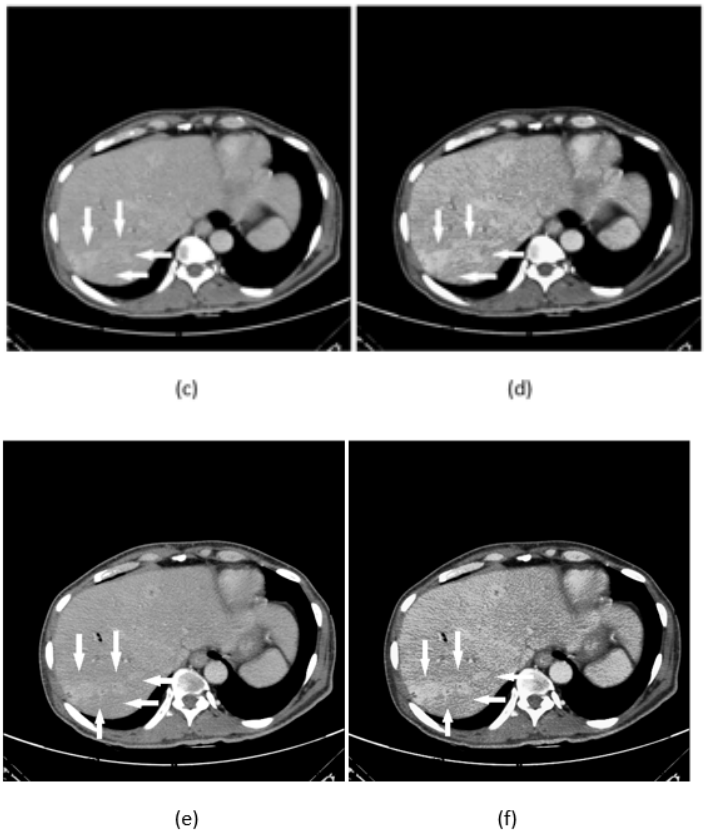

Figure 1: (a), (c), (e) are original CT images of liver and (b), (c), (d) are enhanced CT images of liver

The RMSC, RMSE and AMBE measures are compared for three different contrast enhancement techniques shown in Table 1. Mean and variance of three quantitative measures of 75 CT images are calculated for three techniques i.e. HECVO, HE, CLAHE.

Table 1: Performance comparison of contrast enhancement techniques

Performance measures	HECVO	HE	CLAHE
RMSC	0.2773±0.0888	0.1127±0.02522	0.2892±0.02293
RMSE	7.3407±1.9531	138.7428±128.3671	17.9338±11.2542
AMBE	1.3196±0.5403	132.8548±168.0150	7.1329±13.4152

The RMSC value of HE is lower than HECVO, it implies that HECVO do better contrast enhancement in comparison to HE. The RMSC value of HECVO is slightly lower than CLAHE, but the distortion (RMSE) produced by CLAHE is higher than the HECVO. Contrast enhancement of CT images is required with low distortion, so that image retains its original appearance. Therefore it is clear that HECVO enhances the contrast of image with less distortion in comparison to HE and CLAHE. The AMBE value of HECVO is lowest in comparison to other two techniques, so it can be said that the proposed technique outperforms the HE technique in preserving the mean brightness of the image after processing. CLAHE technique also preserves the mean brightness but HECVO preserves the global outlook of image most significantly. The subjective analysis and quantitative results shows that HECVO enhances the contrast with less distortion and preserves the overall appearance of CT image.

6 Conclusion

The proposed HECVO technique enhanced the contrast of the CT images by preserving its global luminance. After applying HECVO technique the tumor in the CT images are more clearly visible than the original images. Texture of the tissue part of the CT images is enhanced, which is required for better disease diagnosis. Subjective and objective evaluation states that HECVO is suitable algorithm for enhancement of the CT images.

REFERENCES

[1] R.C. Gonzalez, R.E. Woods, Digital Image Processing, 3rd edition, Prentice Hall 2002.

[2] H. Zhu, F.H.Y. Chan, F.K. Lam, Image contrast enhancement by constrained local histogram equalization, Computer Vision Image Understanding, vol. 73, no. 2, pp. 281-290, Feb. 1999.

[3] M. Abdullah-Al-Wadud, Md. Hasanul Kabir, M. Ali Akber Dewan, and Oksam Chae, A Dynamic histogram equalization for image contrast enhancement, IEEE Transactions on Consumer Electronics, Vol. 53, No. 2, pp 593-599, 2007

[4] I. Jafar, H. Ying, Image contrast enhancement by constrained variational histogram equalization, IEEE EIT proceedings pp. 121-125, 2007.

[5] I. Altas, J. Louis and J. Belward, A Variational approach to the radiometric enhancement of digital imagery, IEEE Transactions on Image Processing 4, pp. 845–849, 1995.

[6] P. C. Wu, F. C. Cheng, Y. K. Chen, A weighting mean- separated sub- histogram equalization, National Science Council project NSC 98-2221-E-211-013, IEEE, 2010.

[7] C. Zuo, Q. Chen, X. Sui, Range Limited Bi-Histogram Equalization for image contrast enhancement, Optik 124, Elsevier, pp- 425– 431, 2013.

[8] N. M. Sasi, V. K. Jayasree, Contrast Limited Adaptive Histogram Equalization for Qualitative Enhancement of Myocardial Perfusion Images, scirp, pp- 326-331, 2013.

[9] P. J. Bex and W. Makous, Spatial frequency, phase, and the contrast of natural images, J. Opt. Soc. Am. A 19, 1096-1106, 2002

[10] J. Zimmerman, S. Pizer, E. Staab, E. Perry, W. McCartney, and B. Brenton, Evaluation of the effectiveness of adaptive histogram equalization for contrast enhancement, IEEE Trans. Medical Imaging, pp. 304–312, 1988.

[11] L. O'Gorman, L. S. Brotman, Entropy-Constant Image Enhancement by Histogram Transformation, In the Proceedings of SPIE, vol. 575, pp. 106-113, 1985.

[12] H. Ibrahim, Histogram equalization with range offset for brightness preserved image enhancement, International Journal of Image Processing (IJIP), Volume (5): Issue (5), pp- 599-609, 2011.

[13] Y. Kim, Contrast enhancement using brightness preserving bi-histogram equalization, IEEE Transactions on Consumer Electronics 43, pp. 1–8, 1997.

[14] S. D. Chen and A. R. Ramli, Minimum mean brightness error bi-histogram equalization in contrast enhancement, IEEE Transactions on Consumer Electronics 49, pp. 1310–1319, 2003.

